HPL-2/HP1 and MET-2/SETDB1 bind distinct co-factors that promote heterochromatic foci, gene repression and organogenesis independently of H3K9 methylation

Colin E. Delaney[1], Jia Emil You[1] , Susan M. Gasser[2,3], Jan Padeken[4,5#], and Susan E. Mango[1#]

1. University of Basel Biozentrum, Basel, Switzerland
2. Friedrich Miescher Institute for Biomedical Research, Basel, Switzerland
3. Fondation ISREC, Agora Cancer Research Center, Lausanne, Switzerland
4. Institute for Molecular Biology (IMB), Mainz, Germany
5. Institute for Quantitative and Computational Biosciences (IQCB), Johannes Gutenberg University Mainz, Germany

Corresponding authors

Abstract

Histone post-translational modifications (PTMs) promote genome segregation into heterochromatin and euchromatin by recruiting reader proteins, including HP1 proteins that bind repressive H3 lysine 9 methylation (H3K9me). However, recent studies suggest that H3K9me readers and writers also have PTM-independent activities. Here we examine the PTM-independent roles of the key H3K9 methyltransferase, MET-2/SETDB1, and the *C. elegans* HP1 orthologue, HPL-2, in organogenesis. The two factors co-localize in sub-nuclear foci independently of each other, and their combined loss additively disrupts gene repression and vulval organogenesis. HPL-2 remains functional in the absence of H3K9me, and HPL-2 lacking its H3K9me-binding chromodomain still localizes to heterochromatin foci, restricting vulva formation and repressing developmental genes. While MET-2 requires the disordered protein LIN-65 to form foci and silence genes, HPL-2 functions together with LIN-13, which is bound through HPL-2's chromoshadow domain. In conclusion, HPL-2 and MET-2 repress in parallel on largely H3K9me-independent pathways, requiring distinct cofactors; while H3K9me reinforces both.

Introduction

Cellular differentiation is characterized by the appearance of constitutive heterochromatin, which coalesces into compartments that silence gene expression and safeguard cell-fate [1,2]. The prevailing model, based on studies of repetitive DNA, suggests that heterochromatin is established by methylation of histone H3 at position 9 (H3K9me) [3-5]. Once H3K9me is deposited, reader proteins, such as the highly conserved heterochromatin protein 1, HP1, bind H3K9me2/me3 through their Chromodomains (CD) [6-9]. HP1 binding to nucleosomes, followed by dimerization through its Chromoshadow domain (CSD,[10,11]), compacts chromatin and impedes the transcriptional machinery [12-14]. Propagation of an established domain of heterochromatin through cell division or in terminally differentiated cells requires the histone methyltransferase (HMT) [15,16], which in the case of Su(var)3-9 (hSUV39) can be recruited through its own H3K9me-binding CD [4,17]. These data suggest that cycles of H3K9me deposition and binding stabilize constitutive heterochromatin domains, antagonizing transcription.

The paradigms for H3K9me deposition and propagation arise from its role in repetitive DNA, yet it is now clear that this PTM and its associated modifying enzymes also play an important role in the repression of tissue-specific genes in multicellular organisms, from worms to mammals (reviewed in [18,19]. Indeed, the loss of H3K9me-specific HMTs, which deposit H3K9me through their catalytic SET domains (Suppressor of Variegation, Enhancer of Zeste, Trithorax domain), is associated with aging, altered tumor immunogenicity and defects in tissue differentiation [15,20-29]. These defects correlate with aberrant spatial segregation of heterochromatin and euchromatin [30].

The well-documented pathway for the establishment and propagation of H3K9me in satellite repeats explains its repressive action in these domains, yet recent studies have suggested a more nuanced relationship between the H3K9me mark, its readers and its writers at developmentally controlled genes. For instance, in mouse ES cells, HP1α is recruited independently of H3K9me to a subset of genes and CTCF sites by interaction with the ChAHP complex (CHD4, ADNP, and HP1) [31,32]. Live imaging of single molecules suggests that there exist dynamic, H3K9me-independent interactions between HP1 and nucleosomes [33]. In *Drosophila*, interactions other than the CD-H3K9me interaction are involved in the localization of HP1 to the promoters of genes [34], and HP1A lacking its CD still can associate with heterochromatin [35] in a sequence-independent manner [36]. These examples of PTM-independent interactions stem from studies of cells in culture, and their physiological relevance remains unclear. While evidence is accumulating that point to PTM-independent activities for the readers and writers of H3K9me, it has not been addressed how the PTM-dependent and -independent activities of either HP1 or the HMTs relate to each other, nor how the two pathways reinforce gene repression during development of a multicellular organism. One potential mode of action may involve

the ability of HP1 to phase-separate *in vitro*, and to form condensate-like foci *in vivo* [37-39], although interaction of H3K9me with the nuclear envelope may also play a role [40]. The formation of peripheral nuclear condensates, which we will call "foci", also occurs *in vivo* for the major *C. elegans* H3K9 HMT, MET-2 [28,41]. Here we focus on the relationship between H3K9me, its HMT MET-2/SETDB1 and its reader, the HP1 orthologue HPL-2 in *C. elegans*. While HPL-2 binding has been mapped in whole worms by Chromatin immunoprecipitation (ChIP; [29,42,43], the functional relationship between HPL-2 and H3K9me during cell-fate determination is poorly defined. HPL-2, MET-2/SETDB1 and H3K9me2 map to the same areas of the genome and repress repetitive elements in whole animal ChIP-seq experiments [25,29,42,44]. Nonetheless, overexpressed HPL-2 can bind target loci in embryos lacking all H3K9me[42]. Consistently, HPL-2 acts redundantly with the SETDB1 homolog MET-2 to maintain germline stability and restrict vulval cell differentiation [29,45-47], again suggesting H3K9me-independent functions in development. The MET-2 complex possesses a catalysis-independent function that prevents acetylation of H3K27 and H3K9 in heterochromatin and supports gene repression at certain loci [48]. This correlates with the ability of MET-2 to form dynamic heterochromatic foci independently of H3K9me, but dependent on its largely unstructured co-factor LIN-65/ATF7IP [28,41,49]. HPL-2/HP1 has also been reported to localize to sub-nuclear foci [42,50], yet their relationship to MET-2/SETDB1 foci, transcriptional silencing or tissue differentiation remain unclear.

Here we examine the interdependence of H3K9me, its reader HPL-2/HP1, and writer MET-2/SETDB1, through an analysis of their localization, dynamics, interaction partners, and their ability to silence genes and support appropriate tissue differentiation during *C. elegans* development. We find that while HPL-2 co-localizes with MET-2 in subnuclear heterochromatic foci, the two proteins are recruited to foci independently of each other. This independence is reflected in redundant roles of MET-2 and HPL-2 in gene repression and restricting cell fate. Strikingly, the localization of HPL-2 to heterochromatic foci is not dependent on the recognition of H3K9me by its CD. Instead, HPL-2 localization depends on physical interaction between its CSD and the multi-zinc-finger protein LIN-13. H3K9me binding by the HPL-2 CD plays a minor role in HPL-2-mediated transcriptional repression and is dispensable for vulval cell fate control. Similarly, the ability of MET-2 to control proper vulva determination [45,47] is dependent on its unstructured co-factor, LIN-65, and not on its lysine methylation activity, even when the nuclear localization of MET-2 is artificially maintained. We argue that multivalent protein-protein interactions constitute a generalizable mechanism for heterochromatin function, defining an additional layer of chromatin repression over that mediated by histone PTMs.

Results

MET-2 and HPL-2 colocalize and are independently recruited into heterochromatic foci

Both the HMT MET-2/SETDB1 and the H3K9me-reader HLP-2/HP1 are chromatin factors implicated genetically in vulval cell fate determination [45-47], and both form subnuclear foci [28,41,50,51]. By ChIP, it was confirmed that the two are found on H3K9me-marked repeats that have little or no transcriptional activity, as well as on genes that are repressed in a developmentally controlled manner [29,42,43]. To understand the relationship between H3K9me and its writer and reader, we first asked if endogenous HPL-2 and MET-2 co-localize in foci found in the nuclei of pre-bean stage *C. elegans* embryos (50-100 cells) at the single-cell level. We monitored HPL-2 protein by live imaging of a strain expressing endogenous HPL-2 CRISPR-tagged with mKate2, bearing a 3xFLAG tag in its unstructured hinge region (Figure 1A) [52]. The *hpl-2* gene encodes 2 isoforms [51]. The major isoform accounts for 93% of total protein and exhibits the typical HP1 structure of CD-hinge-CSD, while the less abundant isoform bears an abbreviated CSD and an extended C-terminus (Fig. 1A). The internal HPL-2::mKate2 fusion tags both isoforms and is functional (see below).

As expected, HPL-2::mKate2 was constitutively nuclear and concentrated into subnuclear foci (Fig. 1B). Co-expression of HPL-2::mKate2 with MET-2 endogenously tagged with mNeonGreen [15] confirmed that HPL-2 foci largely colocalized with MET-2 foci at the single-cell level (Fig. 1B). Knockdown of either *met-2* or *hpl-2* led to the loss of green or red fluorescence, respectively, indicating that the signals were specific (Fig. 1C). Surprisingly, the depletion of *met-2* did not alter HPL-2 localization (Fig. 1C). We have previously shown that MET-2 foci form independently of H3K9me using a MET-2 C1237A mutant deficient in catalytic activity (*met-2(catD)*)[48]. Similarly, the foci of HPL-2::mKate2 were not altered in animals expressing *met-2(catD)* (Fig. 1D). Whereas the deletion of *met-2* or *hpl-2* leads to sterility at 26°C, strains expressing HPL-2::mKate2 remained viable and fertile, demonstrating that the protein tag and localization to foci are permissive for HPL-2 function (Fig. 1E).

The second *C. elegans* H3K9 HMT, SET-25 [53,54], which mediates trimethylation of H3K9, and the MBT H3K9me ligand LIN-61 (Koester-Eiserfunke and Fischle 2011), were both dispensable for the formation of either MET-2 or HPL-2 foci (Fig. S1A). A second HP1-like gene in worms, HPL-1, is expressed at much lower levels than HPL-2 in early embryos, being barely detectable until its upregulation in late embryogenesis (Fig. S1B and data not shown, [52]). Loss of *hpl-1* does not exhibit the somatic and germline physiological defects seen in *met-2* or *hpl-2* mutant animals [51], nor does it compromise either MET-2 or HPL-2 foci (Fig. S1A). Therefore, we restricted our focus to HPL-2, its subdomains, and its functional relationship with MET-2.

MET-2 and HPL-2 repress transcription through parallel pathways

We asked if the transcriptional regulatory functions of HPL-2 and MET-2 are independent of each other, like their focus formation, by testing the effect of *hpl-2* and/or *met-2* deletion on transcriptional repression in *C. elegans* embryos. The well-characterized repetitive heterochromatic array *gwIs4* expresses nuclear GFP from a ubiquitously expressed *baf-1* promoter, and is repressed by MET-2, SET-25, and HPL-2 [53,55]. Double deletion of both *met-2* and *set-25* eliminates all detectable H3K9me and led to upregulation of GFP expression from the integrated array (Fig. 2A) [53]. Knockdown of *hpl-2* by RNAi led to a significant increase in GFP expression not only in wild-type embryos, but also in the *met-2Δ set-25Δ* double mutant (Fig. 2A), indicating that HPL-2 harbors a silencing function that is independent of MET-2, SET-25, and H3K9me. At the organismal level, the *met-2Δ* and *hpl-2Δ* double deletion has been shown to lead to a synthetic phenotype for cell-fate restriction in the formation of the vulva, yielding a pronounced multivulval phenotype (Fig. 2B and [45,46]). This phenotype has been extensively characterized in classic synthetic multivulva screens for genes in controlling vulval cell fates (SynMuv; [56]). These results suggest that the two proteins have parallel roles in heterochromatin-mediated repression and in cell fate restriction during vulva differentiation.

For a comprehensive view of endogenous gene expression controlled by MET-2 and HPL-2, we performed RNAseq, comparing the transcriptomes of early embryos in both *met-2Δ* and *hpl-2Δ* mutants. We found 1319 genes up-regulated in *met-2Δ* and 205 genes up-regulated in *hpl-2Δ* (Fig. 2C, FC = 2, FDR = 0.05). Remarkably, not many genes were shared between the two mutant backgrounds (4% of MET-2-controlled and 27% of HPL-2-controlled targets are shared). Comparison of HPL-2 up-regulated genes with those of *set-25Δ* mutants, which specifically lacks H3K9me3, also showed a similar low level of overlap (Fig. S2A). This is consistent with the fact that in embryos SET-25 represses a set of genes that also require MET-2 for their repression (Fig. S2B; and [57]). We have previously shown that the upregulation of genes due to loss of *met-2* methylation activity (*met-2(catD)*) is associated with increased histone acetylation [48]. We therefore tested whether this was true for *met-2Δ* or *hpl-2Δ* embryos, by quantitative immunoblotting whole protein extracts for H3K9ac and H3K27ac. As expected, the levels of acetylated histone H3 were elevated in *met-2Δ* embryos, but we observed no increase in acetylation at these H3 residues in *hpl-2Δ* mutants (Figs. 2D-E). We conclude that although MET-2 and HPL-2 colocalize in heterochromatic foci in embryonic nuclei, as single mutants they derepress distinct cohorts of genes and differentially affect global histone tail acetylation levels. In other words, the reader and writer of H3K9me can repress through distinct pathways.

We next checked for functional redundancy of MET-2 and HPL-2 in transcriptional repression, by performing RNAseq on *met-2Δ hpl-2Δ* double mutant early embryos. Sterile double mutants are maternally rescued, so we employed a fluidic sorting strategy to purify a population of fertile double

mutants from which to isolate embryos (see Methods). We found 928 genes upregulated in *met-2Δ hpl-2Δ* embryos relative to WT (Fig. 2F-G, FC = 2, FDR 0.05). Of these 928 upregulated genes, 543 and 125 genes were upregulated in *met-2Δ* and *hpl-2Δ* single mutants, respectively. However, 352, or 38.2%, of the genes were de-repressed exclusively in the double mutant embryos. We tested a subset of de-silenced genes using qRT-PCR and confirmed synergistic upregulation in *met-2Δ hpl-2Δ* embryos (Fig. 2H), demonstrating that MET-2 and HPL-2 act redundantly to repress this set of genes. We note also that certain repeat families were found to be upregulated only in the double mutant (Fig. S2C). Interestingly, GO term analysis of genes upregulated only in the double mutants showed a prominent enrichment for histone genes (Fig. S2D-E). Taken together, these data show that MET-2 and HPL-2 act redundantly to silence a subset of genes and repeats in worm embryos, yet at the same time they act independently to repress other groups of genes. At only a small fraction of loci do we find that the ablation of either factor derepresses the gene, suggesting that two factors work together, nonredundantly, on this set of promoters. Similarly, in a previous transcriptome study on whole L3 larvae worms that did not analyse the *met-2Δ hpl-2Δ double* mutant, only a fraction of loci derepressed by the loss of H3K9me were also sensitive to loss of HPL-2 [29].

HPL-2 subnuclear foci are reinforced by, but do not require, H3K9me

The transcriptional data suggested that HPL-2 has MET-2- and H3K9me-independent functions in gene repression, in line with earlier work [29,42,43]. We next asked whether HPL-2 foci are independent of H3K9me by deleting both *met-2Δ* and *set-25Δ* [53]. Indeed, HPL-2 still formed foci in the double mutant embryos lacking all detectable H3K9me (Fig. 3A). We conclude that H3K9me is not necessary for HPL-2 focus formation, supporting earlier ChIP data that indicated that HPL-2 can associate with chromatin in a H3K9me-independent manner [29,42,43]. We used automated image analysis to quantify the properties of HPL-2 foci in WT and H3K9me-deficient backgrounds. This revealed that HPL-2 foci are reduced in number, smaller in diameter, less intense and less tightly associated with the nuclear envelope in the absence of H3K9me (WT: mean number 5.7+/- 0.6 and *met-2Δ set-25Δ*: mean 3.6 +/- 0.5 foci/nucleus; p-value: 0.017; size: WT: mean 29.0+/- 0.5 and *met-2Δ set-25Δ*: mean 24.7 +/- 0.6 voxel/foci; p-value: 0.0036; fluorescence intensity of WT: mean 4.6+/- 0.4 and *met-2Δ set-25Δ*: mean 2.9 +/- 0.3 a. u.; p-value: 0.0046) (Fig. 3B-E). Kolmogorov-Smirnov tests (KS) of probability distributions support our conclusion that HPL-2 foci attributes are in fact different between WT and H3K9me-deficient mutants (Table S4). These minor effects observed in the absence of H3K9me cannot be explained by a reduced complement of HPL-2 protein, as both fluorescence intensity and western immunoblots showed no decrease in total HPL-2 protein signal in the *met-2Δ set-25Δ* mutant (Fig. 3F,G). We conclude that HPL-2 foci form in the absence of all detectable H3K9me, although H3K9me reinforces focus assembly and/or positional stability. The fact that HPL-2 foci shifted away from the

periphery in the absence of H3K9me is consistent with previous work showing a role for H3K9me and its interaction with a CD-containing nuclear envelope factor, CEC-4, for anchoring heterochromatin at the nuclear periphery [53,58].

Because MET-2 has a non-catalytic activity in heterochromatin function [48], we asked if MET-2 protein itself, as opposed to the deposition of H3K9me, was important for HPL-2 focus formation, intensity, size and/or association with the nuclear envelope. Animals expressing a catalytically deficient *met-2* (*met-2(catD)*), coupled with *set-25Δ*, showed similar decreases in HPL-2 focus number, size, intensity, and localization at the nuclear envelope compared to *met-2Δ set-25Δ* double mutants, with no decrease in the abundance of HPL-2 (Fig. 3B-G). This result argues that H3K9me rather than MET-2 itself boosts the maintenance and positioning of HPL-2 foci, but heterochromatin focus formation *per se* is not dependent on the PTM. Conversely, the deletion of *hpl-2* did not decrease MET-2::mNeonGreen foci number, intensity, size, nor enrichment at the periphery (*hpl*-2*Δ*, Fig. S3A-E). In conclusion, H3K9me reinforces HPL-2 protein focus size and localization, yet MET-2 forms foci and binds heterochromatin independently of HPL-2 and the PTM. This is remarkable given their co-localization in the same subnuclear foci (Fig. 1).

An HPL-2 mutant unable to bind methyl-lysine retains transcriptional repression, foci-forming competence, and appropriately restricts vulva cell fate

The recognition of H3K9 methylation by HP1 is mediated by its CD [11,59]. To see if HPL-2's ability to localize to chromatin foci in the absence of H3K9me might reflect its interaction with another heterochromatin-associated PTM, such as H3K23me [60], we mutated the conserved binding pocket of the HPL-2 CD, a methylated lysine binding motif that requires a three-amino acid aromatic cage (Fig. 4A) [7,8]. We mutated two phenylalanines of the HPL-2 binding pocket to alanine (F19A and F43A; Fig. 4A) generating a homozygous mutant called *HPL-2(FFAA)*. Analogous mutations in other CD proteins have been previously shown to disrupt H3K9me binding [7,58]. Using an *in vitro* binding assay, we confirmed that this HPL-2(FFAA) double point mutant showed strongly impaired interaction with H3K9me2/me3 (Fig. S4A). Importantly, protein levels of mKate2-tagged HPL-2 were no lower for the HPL-2(FFAA) mutant vs wild-type (Fig. S4B-C).

Despite its inability to bind H3K9me, HPL-2(FFAA) was able to form foci *in vivo* (Fig. 4B). Consistent with the properties of HPL-2 foci in the *met-2Δ set-25Δ* double mutant, the number and average size of foci were decreased in strains expressing HPL-2(FFAA) relative to wild-type HPL-2 (Fig 4C,D). Indeed, H3K9me-binding appears to reinforce the assembly or stability of HPL-2 foci, although focus intensity and peripheral positioning showed only modest effects in the *hpl-2(FFAA)* mutant (vs.

wild-type embryos; Fig. S4D,E). This is consistent with observations in the *met-2Δ set-25Δ* mutant background. Importantly, tagged HPL-2(FFAA) continued to colocalize with the wild-type MET-2, and with the Met-2(catD) proteins (Fig. S4F), suggesting that HPL-2(FFAA) is correctly targeted to heterochromatic foci despite its inability to bind H3K9me.

We then tested the ability of HPL-2 to ensure transcriptional silencing in the absence of a functional CD. If HPL-2 foci have a role in repression, we might expect the *hpl-2(FFAA)* mutant to maintain transcriptional repression of at least a subset of the genes that lose repression in the *hpl-2*Δ embryos. Transcriptome analysis of wild-type, *hpl*-2*Δ*, and *hpl-2(FFAA)* early embryos showed that genes upregulated in *hpl*-2*Δ* embryos indeed remained largely repressed in *hpl-2(FFAA)* embryos (Fig. 4E-F, S4G; FC = 2, FDR = 0.05), indicating that HPL-2 can silence genes in a methyl-lysine-independent manner. This correlates with HPL-2 focus formation. Nevertheless, overall gene expression in *hpl-2(FFAA)* and *hpl-2Δ* correlated (R = 0.64), suggesting that the repression in the *hpl-2(FFAA)* mutant may not be complete (Fig. 4F). We conclude that HPL-2 possesses a silencing function that does not require recognition of H3K9me by its CD.

Given that HPL-2(FFAA) can form foci and repress at least a subset of HPL-2 targets, we next tested whether HPL-2(FFAA) could perform other regulatory functions ascribed to HPL-2. We compared the ability of *hpl-2Δ* and *hpl-2(FFAA)* mutants to support proper vulva differentiation. Both HPL-2 and MET-2 function in adult *C. elegans* vulval development [45], being classified as SynMuvB genes, a genetically defined category that is generally considered to be a single pathway. As single mutants, SynMuvB animals develop a normal vulva, while in combination with a SynMuvA mutation, such as *lin-15A*, the animals produce multiple ectopic pseudovulvae, called the Multi-vulva phenotype (Muv, [56]). This results from the failure to restrict vulval development in the maturing epidermis. We crossed *hpl-2Δ* or *hpl-2(FFAA)* animals into a *lin-15A* mutant background, and, as expected, *hpl*-2*Δ;lin-15A* animals showed high Muv incidence (Fig. 4G). In contrast, the *hpl-2(FFAA);lin-15A* double mutant showed normal vulva development, arguing that developmental lineage specification does not require that HPL-2 bind H3K9me.

Animals with mutations in SynMuvB heterochromatin genes ectopically express germline genes in somatic cells [61-64]. We asked whether this soma-to-germline phenotype was H3K9me-dependent using an endogenous GFP-tagged P-granule protein PGL-1::GFP [15,65]. We imaged the heads of L4 larvae to avoid confounding autofluorescence in the gut and the normal PGL-1 signal in the germline. While deletion of *hpl-2* led to several-fold higher ectopic GFP expression in the heads, animals expressing *hpl-2(FFAA)* retained nearly complete repression of PGL-1 (Figs. 4H). Taken together, these results demonstrate that HPL-2 has an H3K9me-independent function in focus formation, transcriptional repression and vulva cell fate determination.

Given that HPL-2 retained developmental functions independently of H3K9me recognition, we checked whether the catalytic-deficient MET-2 mutant showed similar phenotypes. Indeed, whereas *met-2Δ* showed a strong multivuval phenotype in a *lin-15A* mutant background [45,47], *met-2(catD);lin-15A* animals developed a single vulva (Fig. 5A). Further, *met-20(catD)* animals retained the ability to repress the ectopic expression of PGL-1::GFP in head cells seen in *met-2Δ* mutants (Fig. 5B). Taken together with the *hpl-2(FFAA)* data, we are able to conclude that HPL-2 and MET-2 proteins support normal tissue development and focus formation even when their H3K9me-related functions are compromised.

Physical interaction with distinct complex-forming partners is required for the H3K9me-independent functions of MET-2 and HPL-2

If histone PTMs are not responsible for the developmental and repressive functions of HPL-2 and MET-2, what mechanism(s) enable their regulatory roles in heterochromatin? Both HPL-2 and MET-2 are found in multicomponent complexes, and mass spectroscopy on HP1 chromatin pull-down identified >100 potential ligands for HP1 in metazoans [66]. In contrast, the co-precipitating ligands of MET-2 are LIN-65 and ARLE-14 [28,41], and these are conserved from worms to man (reviewed in [1,18]). The conserved co-factor LIN-65/ATF7IP has large, intrinsically disordered domains (IDR) [28,41]. In the absence LIN-65, MET-2 does not concentrate in the nucleus nor does it form condensate-like foci [41]. LIN-65 itself colocalizes with MET-2 in foci, and LIN-65 localization depends on MET-2, but not H3K9me, given that the number of LIN-65 foci are only marginally affected in the *met-2(catD)* mutant (Fig. 5C,D). A second binding partner of MET-2, ARLE-14/ARL14EP [28,48], is not necessary for focus formation, nor is ARLE-14 a SynMuv gene (Fig. 5E).

We asked to what extent the roles of MET-2 in developmental cell fate decisions depend on LIN-65 [48]. Like *met-2Δ*, deletion of *lin-65* shows a highly penetrant Muv phenotype in the *lin-15A* mutant context (Fig. 5E and [67]) while the *met-2(catD);lin-15A* double does not (Fig. 5A). These findings strengthen the link between focus-forming capacity with cell-fate determination, both being independent of MET-2 HMT activity. LIN-65 has been proposed to cooperate with MET-2 in several ways: one reflects its ability to promote nuclear localization of MET-2, a second to promote nuclear focus formation, while the third would be as a co-factor necessary for HMT activity [28,48]. We have ruled out that MET-2 HMT activity is essential for vulval cell-fate restriction and/or germline gene repression: both are independent of H3K9me (Fig. 5A,B). To see if we could bypass the requirement for LIN-65 by targeting MET-2 to the nucleus artificially, we tagged MET-2 with a nuclear localization signal (NLS; [28]). This tag is sufficient to maintain a strong nuclear enrichment of MET-2 in the absence of *lin-65,* but

does not support focus formation [48]. Whereas *NLS::met-2* behaved like wild-type MET-2 did not act as a SynMuv mutant on its own, *NLS::met-2* could not support normal vulval development in the absence of LIN-65 (Fig. 5F). Fertility assays also showed that *NLS::met-2* failed to rescue the low level of fertility of *lin-65Δ* in double mutant animals (Fig. 5G). Taken together, these results indicate that the binding of LIN-65 to MET-2 is needed to stabilize subnuclear foci and fulfill developmental cell-fate decisions (vulva, germline stability), which cannot be compensated for by targeting a catalytically active MET-2 to the nucleus. Thus, the LIN-65-MET-2 complex enables heterochromatic focus formation, cell fate restriction and gene repression, independently of H3K9me and HPL-2. We note that LIN-65's IDRs create the potential for higher-order interactions with nucleic acid as well as proteins, which may contribute to biomolecular condensates [68,69].

To relate this PTM-independent behavior of MET-2 to PTM-independent HPL-2 functions, we examined one of HPL-2's relevant ligands, the lineage determining factor LIN-13, a C2-H2 zinc finger-containing protein that binds the HPL-2 CSD through a motif in its N-terminus [50]. The LIN-13-HPL-2 complex has already been implicated in nuclear focus formation and vulva development [50], which we confirm in Fig. 6A. To examine whether MET-2 and/or HPL-2 foci are interdependent – that is, cross-regulated by either of the factors' co-factors, LIN-65 or LIN-13, we first examined HPL-2 foci in a *lin-65 k*nockdown. Whereas MET-2 foci disappeared, with MET-2 showing a non-nuclear dispersion in the absence of LIN-65, HPL-2 foci remained visibly unchanged (Fig. 6A). Knockdown of *lin-13* led to the depletion of HPL-2 foci, as previously reported [50], but we show that LIN-13 was dispensable for MET-2 foci formation (Fig. 6A). These data confirm that HPL-2 and MET-2 locate to the same foci independently of each other (Fig. 1), and show that localization is also independent of the other factor's required cofactor, LIN-13 and LIN-65, respectively.

To understand how LIN-13 contributes to HPL-2 function in vulval cell fate, we examined the HPL-2-LIN-13 interaction in greater detail. A previous study reported that HPL-2 and LIN-13 bind directly in yeast two-hybrid studies and that over-expressed proteins can be co-precipitated from worm extracts [50]. We performed immunoprecipitation of endogenously FLAG-tagged HPL-2::mKate2 followed by mass spectrometry (IP-MS) to characterize HPL-2 interactions in embryo lysates. LIN-13 peptide intensities were indeed enriched in the HPL-2::mKate2 strain relative to the N2 untagged control (Fig. 6B). Consistent with a model of independent recruitment, HPL-2 pulldowns did not enrich for MET-2, nor did previous MET-2 pulldowns enrich for HPL-2 (data not shown and [28,41,48].

The data above demonstrating that the HPL-2-FFAA mutant suffices for vulval development and transcriptional repression argues against an essential role for the chromodomain. In contrast, two-hybrid interaction studies suggest that the HPL-2 CSD suffices for binding LIN-13 [50,56,70,71]. To test which domains were necessary for HPL-2 function, we used CRISPR to delete the entire chromodomain (aa

19-71, *ΔCD*) or the portion of the CSD shared between both short and long isoforms that contains the conserved residues necessary for binding the PXVXL motif [11] in the FFAA background (aa 112-151, *ΔCSD*) (Fig. 6C).). To characterize these domain mutants, we examined the interaction with LIN-13 via immunoprecipitation of the HPL-2 mutants followed by mass spectrometry (IP-MS). While LIN-13 remained enriched in ΔCD mutants to a similar extent as WT, LIN-13 enrichment was lost in *FFAAΔCSD* embryos (Fig. 6D). Therefore, the HPL-2 CSD is necessary for interaction with LIN-13 in vivo, in the absence of methyl-lysine binding. Consistent with the *hpl-2(FFAA)* point mutants, the HPL-2 enrichment in foci was retained in embryos lacking the chromodomain but lost in *FFAAΔCSD* embryos, confirming that LIN-13-dependent physical interaction mediated by the CSD is necessary for HPL-2 foci formation (Fig. 6E,F).

To see how this result ties into developmental functions, we tested the relevance of the various HPL-2 domain mutations for gene repression and vulva specification. Whereas *hpl-2ΔCD;lin-15A* animals showed a low penetrant Muv phenotype (8.2%, Fig. 6G), animals lacking methyl-lysine binding residues (FFAA mutant) and the LIN-13-binding motif (*ΔCSD*) showed highly penetrant defects in vulva development (90.9%, Fig. 6G). We used qRT-PCR to interrogate genes identified by RNAseq as being repressed in an HPL-2-dependent manner. Deletion of the chromodomain had only modest effects on transcription, while HPL-2(FFAA-*ΔCSD)* embryos upregulated genes similar to *hpl-2Δ* embryos (Fig. 6H). Therefore, we conclude the HPL-2 CSD mediates interactions with its multivalent binding partner LIN-13 to drive foci formation, repress transcription, and promote proper tissue differentiation.

Discussion

In this study, we reveal independent roles for two central players in the formation of H3K9me-marked heterochromatin, the H3K9 HMT MET-2/SETDB1 and the paradigmatic heterochromatin ligand, HPL-2/HP1. We find that each harbors PTM-dependent and PTM-independent functions in gene repression during cell differentiation, and that the PTM-independent functions are critical for organogenesis (Figure 7). Recent studies have suggested that several histone-modifying enzymes retain partial function in the absence of their enzymatic activities, just as PTM-independent functions have been attributed to HP1 [72]. However, it was unclear how these sets of factors (the readers and writers of histone modifications) interact, particularly in the context of PTM-independent pathways of gene control. We show here that in *C. elegans* the H3K9me ligand HPL-2/HP1 and its writer, MET-2/SETDB1, function largely independently of one another to silence distinct groups of genes (Fig. 2G), yet they can act redundantly, even in an additive manner, to silence other loci. The genes repressed in parallel

by both MET-2 and HPL-2 appear to be particularly relevant to heterochromatic silencing in developmental cell fate decisions because the combined loss of the PTM-independent focus forming functions of MET-2 and HPL-2 leads to the generation of multiple pseudovulvae in the soma, as well as germline lethality.

The PTM-independent functions of MET-2 and HPL-2 depend on physical interactions with distinct multivalent binding partners, the multiple zinc-finger protein LIN-13 for HPL-2 and the intrinsically disordered LIN-65/ATF7IP for MET-2/SETDB1 (Fig. 7). These interactions are also necessary for the independent localization of HPL-2 and MET-2 in heterochromatic foci, but they do not cross-target ligands. We have used point mutations and domain deletion alleles to demonstrate that the HPL-2 CSD, which is required for interaction with LIN-13, is crucial to maintain gene repression and proper organogenesis (Fig. 6). Similarly, a catalytic-deficient MET-2 is able to support focus formation, selective gene repression and proper organogenesis, as long as it can bind its unstructured cofactor LIN-65 (Fig. 5). It is important to note that the histone modification H3K9me is not essential for the concentration of either factor into foci, although it does contribute to the robustness and peripheral distribution of HPL-2 clusters. Our work argues that protein-protein interactions supersede the role of H3K9me recognition by HPL-2 in gene repression relevant to worm development (Fig. 7), and that focus formation coincides with these crucial protein-protein interactions. We believe these data provide compelling evidence that heterochromatin foci—that is, non-membrane-bound compartments that concentrate silencing factors—participate in PTM-independent repression that has a demonstrable role in organogenesis.

The histone code hypothesis argues that a combinatorial crosstalk between post-translational modifications of histones regulates chromatin function, including the selective expression of genes [73]. In particular, it has been well established that both the writers and readers of H3K9 methylation help stabilize and repress repetitive elements and transposons, in large arrays that flank centromeres and the rDNA [25,29,44,74-77]. In fact, the expression of transposons and transcripts from satellite and simple repeats is the most striking feature arising from the loss of H3K9me [25,29,44,75-78]. Importantly, in *Drosophila,* Penke et al (2016) replaced the acceptor lysine 9 in histone H3 with arginine and found that a small number of animals could develop to adulthood, but piRNA clusters, transposons and other repeats were strongly upregulated[78]. However, in addition to the role of H3K9me and its readers in the organization of repetitive DNA, extensive evidence now documents H3K9me on the promoters of pluripotency and tissue-specific genes that are silenced during differentiation [15,42,44,74-77]. Indeed, loss of the H3K9-HMT, even after terminal tissue differentiation, leads to gene derepression and loss of tissue integrity and cell-fate commitment [18,27].

The paradigm of a targeted recruitment of the H3K9me HMT through dsRNA and a propagation of the mark through reader-writer-PTM interactions was established in *S. pombe* [3], and appears to be relevant for the repression of repetitive sequences in general. However, an increasing number of examples, including this work, uncouples the PTM writer from its histone mark, particularly in the regulation of unique genes in a developmental context. We show this for both the major H3K9 HMT, MET-2, and the canonical H3K9me reader, HPL-2. Analogous examples are found in other species: in *Drosophila*, for instance, the histone acetyltransferases (HATs) CBP and Gcn5 are required for zygotic genome activation, yet can perform their essential role in development independent of their acetylation activity [79]. In mammalian cells, p300 plays an important role in transcription coactivation, but chromatin interactions have been reported to be opposed by its HAT activity [80]. Use of chemical inhibitors of HAT activity has strengthened the evidence for acetylation-independent functions of CBP [81]. Among methyltransferases, mammalian MLL3 and MLL4 have been shown to promote enhancer activation independent of their H3K4 HMT activity [82]. Finally, the mammalian H3K9 HMT G9a can function in transcriptional repression independent of its enzymatic activity by recruiting DNA methyltransferases [83,84]. Earlier work in worms showed that the catalytic-deficient MET-2(catD) enzyme mitigates germline and somatic phenotypes associated with *met-2Δ*, and served to prevent histone hyperacetylation and silence a subset of MET-2-repressed genes (Fig. 5, [48]). Analogously, a subsequent study in mouse showed that SETDB1 bearing the homologous C1243A catalytic deficient mutation rescues defects in mouse stem cell pluripotency caused by simultaneous triple-deletion of HP1α/HP1β and HP1γ [85]. Clearly, many histone modifying enzymes, including MET-2/SETDB1, can influence chromatin organization independently of their catalytic activity.

Essential to the PTM-independent functions of MET-2 in *C. elegans* is the conserved cofactor LIN-65/ATF7IP, which enables heterochromatic focus formation and cell fate restriction (Fig. 5). This is not simply because LIN-65 promotes the nuclear enrichment and methylation activity of MET-2 (Fig. 5); rather, the complex formed by MET-2 and LIN-65 functions in vulva cell fate determination in the absence of H3K9 methylation, and functions independently of HPL-2. We have shown that although H3K9me enhances the robustness of HPL-2 foci and the efficiency of gene repression, the LIN-13 interaction is more important, being essential for both PTM-dependent and -independent functions. This is consistent with a report from *Drosophila,* showing that H3K9me enhances, but is not required for, HP1A accumulation at promoters and pericentromeric regions [34,86].

We have identified the domains of HPL-2 that are critical for its repressive role in development. HP1 proteins consist of a H3K9me-reader CD, a flexible hinge region, and a CSD that enables homo- and heterodimerization with binding partners[12,72]. In mammals, the CSD leads to the recruitment of Suvar3-9 and Suv420H2, leading to more repressive H3K9me and H4K20me3, respectively [87,88]. Several

CSD interactions with chromatin-associated factors have been reported, including CAF-1, a nucleosome chaperone, and KAP-1, which forms a complex with SETDB1 and with KRAB zinc finger proteins [72,89-92]. We show here that the CSD is required both for the concentration of HPL-2 into foci and for the crucial regulatory interaction of HPL-2 with LIN-13, that is, for the repression of germline genes and specification of a single vulva during worm development. Surprisingly, the HPL-2 CD played only a minor role in cell fate, transcription, and protein foci dynamics, perhaps due to the redundancy of the PTM-dependent pathway with LIN-61, an MBT-domain protein that also binds H3K9me [93].

How do protein complexes control the functional compartment-forming activity of nuclear chromatin? One possible mechanism may be by forming a scaffold that attracts multiple agonists or antagonists to gene activation. For instance, p300 is proposed to act as a scaffold, stimulating transcription by simultaneously recruiting multiple transcription factors [80]. Some of this activity may be attributed to IDRs that trigger condensation when sufficiently concentrated [94]. For example, histone acetylation reader BRD4 forms condensates through its IDR, yet the biophysical properties of these foci are altered by the presence of its ligand acetyl-lysine [39,95]. While IDRs are unstructured, they have unique biochemical attributes like electrostatic charge and primary sequence that allow for both nucleic acid binding and protein sequestration [38,96-98]. Our data and that of others demonstrate that the HP1 homolog HPL-2 forms foci *in vivo* in a manner independent of H3K9me, but dependent on its CSD-mediated interaction with LIN-13. The 24 zinc fingers and LIN-35/Rb binding motif of LIN-13 could in turn serve as a scaffold that promotes multivalent HPL-2 interactions [50]. Similar to IDRs, these are thought to be drivers of condensate formation, possibly through RNA or DNA interaction. We note that LIN-13 is a multiple Zn-finger protein, and that other such proteins, notably TFIIIA, bind RNA as well as DNA [99]. One could imagine that HPL-2-LIN-13 may trap nascent RNAs for nuclear degradation as an alternative, or complementary, mode of gene repression [57,100].

We note that MET-2/SETDB1 also has an unstructured N-terminus, which allows MET-2 to bind LIN-65/ATF7IP, a factor with an extensive IDR; moreover, the interaction of MET-2 with LIN-65 coincides with condensate-like focus formation. Given that LIN-65/ATF7IP and MET-2/SETDB1 complex is well conserved in mammals, this pathway is most likely conserved [28,29,41,48,49,101-103]. That said, it is possible that condensate formation may be more relevant in species in which the H3K9me HMT lacks a PTM-reading motif, as in the *C. elegans* MET-2 protein. In contrast, Su(var)3-9 (hSUV39) has its own H3K9me-binding CD [17].

We note that earlier studies suggested that LIN-13, MET-2, and HPL-2 work together with other heterochromatin-associated proteins to prevent DNA damage and germline apoptosis [29]. The novelty of our study is to show that LIN-13, HPL-2 and the major H3K9 HMT, MET-2, act on distinct PTM-independent pathways to repress many of the same target genes, including germline and vulval cell

lineage genes [61-64]. We do not exclude that the two factors act together, i.e. on a common pathway, for repeat repression and genome stability mostly likely through H3K9 methylation. Yet, we show here that multivalent protein-protein and protein-chromatin interactions, which coincide with focus formation and contribute to PTM-independent regulation of transcription, are an integral part of the chromatin playbook that is crucial for restricting cell fate in development.

Methods

Strains and maintenance

Strains used for these studies are documented in Supplementary Table 1. "Some strains were provided by the CGC, which is funded by NIH Office of Research Infrastructure Programs (P40 OD010440)." Animals were cultured at 20°C unless otherwise indicated. Embryos were isolated either by dissection or by standard bleaching protocols. RNA interference (RNAi) knockdown of genes was achieved as previously described [104,105]. Synchronized L1 animals were fed HT115 E coli expressing double stranded RNA targeting the indicated gene on nematode growth media plus 1 mM IPTG and 100 µg/mL carbenicillin. RNAi targeting *lin-13* was a gift from Francesca Palladino (CNRS Lyon).

Transgenesis

Targeted substitutions and deletions were created in endogenous gene loci using CRISPR-Cas9 exactly as previously described [106]. AltR Cas9 and tracrRNA (IDT) were used. AltR crRNAs were synthesized by IDT. Edit-specific crRNA sequences and Homology Directed Repair template sequences (IDT) are provided in Supplementary Table 2.

Live microscopy

Imaging was performed at 20°C. 2D DIC images were captured using a Zeiss Axio Zoom V16 and Zeiss Axiocam 503 mono camera with ZEN 2.6 blue edition software. Fluorescent 3D imaging were obtained using an Olympus IX83 microscope outfitted with a Yokogawa CSU-W1 confocal 50 µm spinning disk, and Hamamatsu ORCA-Fusion sCMOS camera. Images were deconvolved with the Huygens Remote Manager. Automated image segmentation analysis of nuclei and foci was performed with Knime [107].

Developmental phenotypes

Fertility assays: L4 animals grown at the indicated temperature were placed one (25°C) or three (26°C) animals per plate. Egglayers were transferred to fresh plates every 24 hr for the duration of egglaying, after which total progeny were counted.

SynMuv assays: Gravid adults were allowed to lay eggs for several hours, then removed. Laid eggs were allowed to mature to day 1 adults for 72 hr at 20°C, at which time animals were visually scored for the presence or absence of abnormal vulva development.

Immunoprecipitation-mass spectrometry (IP-MS)

Immunoprecipitations were performed as previously reported [41]. All steps were performed on ice or 4°C. Briefly, mixed embryos isolated by bleaching from 100,000 day 1 adult animals were homogenized

in TAP buffer (150 mM NaCl, 20 mM Tris-HCl, pH 7.5, 0.5% NP-40, 1 mM EDTA, 10% glycerol, 2× cOmplete-EDTA-free protease inhibitors (Roche), 1× Deacetylase Inhibitor (Active Motif), and 1 mM DTT) using 0.5 mm Glass Globules (Roth) and a Fast Prep-24 homogenizer (MP Biomedicals). Lysates were sonicated in 14 cycles of 15 s on, 30 s off using a Bioruptor Plus (Diagenode). Lysates were cleared via centrifugation at 21,000g for 10 min at 4°C. Anti-FLAG-M2 magnetic beads (Sigma) pre-washed in TAP buffer were added to 5 mg protein lysate and rotated overnight at 4°C. Beads were washed in TAP buffer 4 x 15 min, then 3 times with MS wash buffer (20 mM Tris-HCl, pH 7.5, 150 mM NaCl) to remove detergents.

Resin was resuspended in elution buffer (5% SDS, 10mM TCEP, 0.1 M TEAB), incubated for 10 min at 95°C and transferred into a new tube. Proteins were alkylated in 20 mM iodoacetamide for 30 min at 25°C and digested using S-Trap™ micro spin columns (Protifi) according to the manufacturer's instructions. Briefly, 12 % phosphoric acid was added to each sample (final concentration of phosphoric acid 1.2%) followed by the addition of S-trap buffer (90% methanol, 100 mM TEAB pH 7.1) at a ratio of 6:1. Samples were mixed by vortexing and loaded onto S-trap columns by centrifugation at 4000 g for 1 min followed by three washes with S-trap buffer. Digestion buffer (50 mM TEAB pH 8.0) containing sequencing-grade modified trypsin (1/25, w/w; Promega) was added to the S-trap column and incubate for 1h at 47 °C. Peptides were eluted by the consecutive addition and collection by centrifugation at 4000 g for 1 min of 40 ul digestion buffer, 40 µL of 0.2% formic acid and finally 35 µL 50% acetonitrile, 0.2% formic acid. Samples were dried using a Speedvac and stored at -20 °C until further use.

Dried peptides were resuspended in 0.1% aqueous formic acid and subjected to LC–MS/MS analysis using a Orbitrap Fusion Lumos Mass Spectrometer fitted with an EASY-nLC 1200 (Thermo Fisher Scientific) and a custom-made column heater set to 60°C. Peptides were resolved using a RP-HPLC column (75µm × 36cm) packed in-house with C18 resin (ReproSil-Pur C18–AQ, 1.9 µm resin; Dr. Maisch GmbH) at a flow rate of 0.2 µL/min. The following gradient was used for peptide separation: from 5% B to 12% B over 5 min to 35% B over 40 min to 50% B over 15 min to 95% B over 2 min followed by 18 min at 95% B. Buffer A was 0.1% formic acid in water and buffer B was 80% acetonitrile, 0.1% formic acid in water.

The mass spectrometer was operated in DDA mode with a cycle time of 3 seconds between master scans. Each master scan was acquired in the Orbitrap at a resolution of 120,000 FWHM (at 200 m/z) and a scan range from 375 to 1600 m/z followed by MS2 scans of the most intense precursors in the linear ion trap at "Rapid" scan rate with isolation width of the quadrupole set to 1.4 m/z. Maximum ion injection time was set to 50ms (MS1) and 35 ms (MS2) with an AGC target set to 1e6 and 1e4, respectively. Only peptides with charge state 2 – 5 were included in the analysis. Monoisotopic

precursor selection (MIPS) was set to Peptide, and the Intensity Threshold was set to 5e3. Peptides were fragmented by HCD (Higher-energy collisional dissociation) with collision energy set to 35%, and one microscan was acquired for each spectrum. The dynamic exclusion duration was set to 30s.

The acquired raw-files were searched using MSFragger (v. 4.0) implemented in FragPipe (v. 21.1) against a C. elegans database (consisting of 26584 protein sequences downloaded from Uniprot on 20220222) and 392 commonly observed contaminants spiked with the sequence of mKate2 using the "LFQ-MBR" workflow. Quantitative data was exported from FragPipe and analyzed using the MSstats R package v.4.13.0. (https://doi.org/10.1093/bioinformatics/btu305). Data was normalized, imputed using "AFT model-based imputation" and q-values for pairwise comparisons were calculated as implemented in MSstats.

in vitro binding assay

Embryo lysed in IVB buffer (30mM Tris-HCl pH 7.5, 600 mM NaCl, 1 mM EDTA pH 8.0, 5% glycerol, 1% Triton X-100, 2X cOmplete-EDTA-free protease inhibitors (Roche), and 1 mM DTT) [108] were processed exactly as in immunoprecitation above. Dynabeads™ MyOne™ Streptavidin C1 (Invitrogen) were rotated with 4X excess biotinylated H3 tail peptides (Anaspec) in TAP buffer for 4 hr at 4°C. Beads were then washed 3X in IVB buffer and stored on ice prior to use. Equivalent amounts of protein were distributed to tubes containing peptide-bead complexes and rotated overnight at 4°C. Beads were washed 4X with IVB buffer, then resuspended in TAP buffer and stored at -20°C until use.

Western blotting

10 µg of total protein from embryo lysates was separated on Criterion XT Bis-Tris gels (Bio-Rad) using either MES or MOPS buffer (Invitrogen). Proteins were transferred using a Trans-blot semi-dry system and Trans-blot Turbo Midi 0.2 µm PVDF pre-cut membranes (Bio-Rad). Membranes were blocked in either PBS + 0.5% Tween-20 (PBST) containing 5% milk (Sigma) or Protein-free blocking buffer (Pierce) depending on the antibody of interest. Primary antibodies include 1:10,000 mouse anti-H3K9ac and 1:10,000 mouse anti-H3K27ac (gifts of H. Kimura), 1:10,000 rabbit anti-H2B (Abcam ab1790), and 1:25,000-1:50,000 mouse anti-FLAG M2 conjugated to HRP (Sigma). Blots were rotated overnight at 4°C, washed three times in PBST, blocked again and exposed to HRP-conjugated secondary antibodies, when applicable, for 1 h at RT. Secondary antibodies include 1:100,000 goat anti-mouse IgG HRP (Jackson ImmunoResearch 115-035-146) or 1:100,000 goat rabbit IgG HRP (Jackson ImmunoResearch 111-035-144). We used Immobilon HRP substrate (Millipore) and detected signal using a Fusion FX camera operated with Fusion FX7 Edge Software (Vilber).

RNA isolation

RNA was extracted from early embryos from synchronized cultures grown at 20°C as reported previously using Trizol (Invitrogen) [25]. For in *met-2Δ hpl-2Δ* double mutant embryos, heterozygotes with a GFP + balancer were expanded. Non-fluorescent L1 progeny—maternally rescued, homozygous double mutant animals—were selected using a COPAS Biosort (Union Biometrica), from which early embryos were harvested. Embryos were freeze cracked five times, then RNA was extracted with choloroform followed by isopropanol precipitation. Further purification was performed with the RNA Clean and Concentrator kit (Zymo).

qPCR

cDNA was synthesized using Maxima H Minus Reverse Transcriptase (ThermoFisher) according to manufacturer's instructions. 1 ug RNA was primed using Oligo(dT)20 primer (Invitrogen). Reactions were performed using the PowerUp SYBR Green Master Mix (Applied Biosystems). Ct values were determined with Mastercycler EP realplex software. Housekeeping gene pmp-3 was used for normalization [109] and relative expression was calculated with the ΔΔCt method [110].

RNA sequencing

Libraries were produced using the Stranded Total RNA Prep Ligation with Ribo-Zero Plus Kit (Illumina). rRNA was depleted using the Ribo-Zero Plus kit supplemented with custom made C. elegans specific rDNA oligos (IDT). Libraries were profiled in a DNA 1000 Chip on a 2100 Bioanalyser (Agilent technologies) and quantified using the Qubit 1x dsDNA HS Assay Kit, in a Qubit 4.0 Fluorometer (Life technologies). Equimolar amounts of indexed libraries were pooled and sequenced on a NextSeq 2000 (Illumina). Reads were analysed as described previously [48]. Adapter were trimmed using Trimmomatic v0.39. Reads were aligned to the C. elegans genome (ce10) with the R package QuasR v1.44.0, (www.bioconductor.org/packages/2.12/bioc/html/QuasR.html). The command "proj <- qAlign("samples.txt","BSgenome. Celegans.UCSC.ce10", splicedAlignment=TRUE)" instructs hisat296 to align using default parameters, considering unique reads for genes and genome wide distribution. Count Tables of reads mapping within annotated exons in WormBase (WS220) were constructed using the qCount function of the QuasR package to quantify the number of reads in each window (qCount(proj, GRange_object, orientation="same")) and normalized by division by the total number of reads in each library and multiplied by the average library size. Transformation into log2 space was performed after the addition of a pseudocount of 12 to minimize large changes in abundance fold change (FC) caused by low count numbers. The EdgeR package v4.2 was applied to select genes with differential transcript abundances between indicated genotypes (contrasts) based on false discovery rates (FDR) for genes (FDR <0.05 and log2 fold change >1 for up regulated genes and <-1 for down

regulated genes). Replica correlations are shown in Fig SXXX of GO-Terms were extracted from wormbase.org and the GO-Term and KEGG pathway enrichment analysis was performed using the gprofiler2 package (v 0.2.3) as an interface to g: Profiler [111].

Acknowledgements

We would like to thank the Imaging Core facility (IMCF Biozentrum), the Proteomics core facility members (Biozentrum, University of Basel) and the Genomics Core Facility (IMB, Mainz) for helpful discussions and technical assistance; and Iskra Katic at Fredrich Miescher Institute (FMI) for providing sound advice and technical support for fluidic sorting of animals. Jan Padeken is associated with the SFB 1551 Project No. 464588647 of the DFG (Deutsche Forschungsgemeinschaft). SMG thanks the ERC AdvGrant Epiherigans. SEM is supported by Univ of Basel and SNF 10001070. CD was supported by the Novartis Stiftüng für medizinischbiologishe Forschung.

Authors' Contributions.

CED: Conceived the project, performed experiments, data curation, formal analysis, methodology, Investigation: data in figures, Writing: original draft, review, editing.

JEY: Investigation: performed experiments

SG: Funding acquisition, paper writing, review, editing

JP: Investigation: data in figures; Writing: review, editing; funding acquisition

SEM: conceptualization; writing: review, editing, supervision; funding acquisition, project administration

Availability of data and materials

RNA seq results are available online.

Declaration of interests

The authors declare no competing interest

Figure Legends

Fig. 1. MET-2 and HPL-2 colocalize in heterochromatin foci independently of each other. (**A**) Schematic of HPL-2 protein isoforms expressed from the same locus, with isoform percentage of total protein indicated in parentheses as determined by Western blot (mean, N = 3). Red triangle = mKate2::3xFLAG insertion site in the hinge domain. (**B**) Representative images *C. elegans* embryos at the 50-100 cell stage expressing endogenously tagged MET-2::mNeonGreen with endogenously tagged HPL-2::mKate2. Dashed oval indicates the circumference of the embryo. Dashed boxes indicate example nuclei enlarged below. Scale bar, 5 µm. N = 3, n = 30. **(C)** Representative images of embryos co-expressing MET-2::mNeonGreen with HPL-2::mKate2 treated with *met-2*, or *hpl-2* RNAi or empty vector control. Scale bar, 5 µm. N = 3, n = 30. **(D)** Representative images of MET-2::mNeonGreen co-expressed with HPL-2::mKate2 in WT, *met-2(catD)*, and *hpl-2(FFAA)* backgrounds. Scale bar, 5 µm. N = 3, n = 30. **(E)** Mean progeny per worm at 26°C in WT, *hpl-2Δ*, and *hpl-2::mKate2::3xFLAG*. N = 2, n = 60 egg focal sections. Bars indicate mean value of each genotype.

Fig. S1. MET-2 and HPL-2 foci formation does not require other genes implicated in heterochromatin. (**A**) Representative images of embryos co-expressing MET-2::mNeonGreen with HPL-2::mKate2 treated with the indicated RNAi or empty vector control. Scale bar, 5 µm. N = 3, n = 30. (**B**) Representative images of embryos expressing either HPL-1::mKate2 or HPL-2::mKate2. Dashed oval indicates the circumference of the embryo. Inset shows overexposed region highlighted in the dashed box. Scale bar, 5 µm. N = 3, n = 75.

Fig 2. H3K9me and HPL-2 act independently to repress transcription. (**A**) Representative images of whole embryos at 50-100 cell stages, and quantitation of GFP signal from the *gwIs4* heterochromatic array. N = 3, n(embryos): WT vector = 99, WT *hpl-2* RNAi = 134, *met-2Δ set-25Δ* vector = 39, *met-2Δ set-25Δ hpl-2* RNAi = 53. *$p < 3x10^{-4}$, **$p < 10^{-9}$ by one-way ANOVA, followed by Bonferroni post hoc test. (**B**) Representative images of vulva development in adult animals. Normal vulvae = circle, multiple pseudovulvae = arrowheads. Quantitation was reported previously [45]. (**C**) Venn diagram showing overlap of *hpl-2Δ* and *met-2Δ*-derepressed genes measured by RNAseq. N = 3, FC > 2, FDR < 0.05. (**D**) Representative western blot and quantitation of acetylated H3K9 normalized to histone H2B in WT, *hpl-2Δ* and *met-2Δ* single mutants. *N* = 4. *p = 0.034 by two-sided *t*-test. (**E**) Representative western blot and quantification of H3K27 acetylation normalized to histone H2B in WT, *hpl-2Δ* and *met-2Δ* single mutants. *N* = 3. *p = 0.014 by two-sided *t*-test. (**F**) Venn diagram and (**G**) heat map showing up-regulated genes in *met-2Δ hpl-2Δ* double mutant early embryos measured by RNAseq, and the subset of genes independently observed to be de-repressed in *hpl-2Δ* and/or *met-2Δ* single mutant early embryos. N = 3, FC > 2, FDR < 0.05. (**H**) qRT-PCR of a subset of *met-2Δ hpl-2Δ* double mutant up-

regulated genes or the control gene *lmn-1*. Bars show means while dots indicate individual measurements. N = 3.

Fig S2. MET-2 and HPL-2 silence repeats and a subset of genes in a redundant fashion. Venn diagrams showing overlap of *set-25Δ* mutant upregulated genes with (**A**) *hpl-2Δ* mutant or (**B**) *met-2Δ* mutants upregulated genes measured in independent RNAseq experiments. N = 3, FC > 2, FDR < 0.05. (**C**) Heat map showing *met-2Δ hpl-2Δ* up-regulated repeat families measured by RNAseq, and the subset of genes independently observed de-repressed in *met-2Δ* early embryos. N = 3, FC > 2, FDR < 0.05. (**D**) GO Terms of genes upregulated in *met-2Δ hpl-2Δ* RNAseq vs. WT. (**D**) Heat map showing *met-2Δ hpl-2Δ* up-regulated histone genes, with color code as in (C).

Fig 3. HPL-2 forms nuclear foci independently of H3K9 methylation. (**A**) Representative live images of HPL-2::mKate2::3xFLAG in WT, *met-2Δ set-25Δ*, or *met-2(catD) set-25Δ* embryos. Scale bar, 5 µm. N = 3, n = 30. Quantification of HPL-2::mKate2 foci from (A) measuring (**B**) foci number per nucleus, (**C**) size of foci, (**D**) mean foci intensity per nucleus, and (**E**) Quantification of HPL-2::mKate2 foci distance to the nuclear periphery. Panel (**F**) shows a representative western blot of HPL-2::mKate2::3xFLAG protein levels in WT, *met-2Δ set-25Δ*, or *met-2(catD) set-25Δ* embryos. N = 4. And (**G**) shows mean nuclear intensity of HPL-2 in the same mutants. *P-values (*met-2Δ set-25Δ* , *met-2(catD) set-25Δ* vs WT): (B) $p = 0.017$, $p = 6.0 \times 10^{-3}$, (C) $p = 4.2 \times 10^{-3}$, $p < 3.6 \times 10^{-3}$, (D) $p = 3.1 \times 10^{-4}$, $p = 4.6 \times 10^{-3}$, (E) $p = 2.1 \times 10^{-13}$, $p < 2.2 \times 10^{-16}$, (G) not significant, by one-way ANOVA, followed by Tukey post hoc test. KS-test statistics reported in Table S4.

Fig S3. MET-2 foci form independently of *hpl-2*. (**A**) Representative live images of MET-2::mNeonGreen in WT and *hpl-2Δ* embryos. Scale bar, 5 µm. N = 3, n = 30. Quantification of MET-2::mNeonGreen foci (**B**) number, (**C**) intensity, (**D**) size, and (**E**) distance to the nuclear periphery from data in (A). *P-values (*hpl-2Δ* vs WT): (B) not significant (NS), (C) NS (D) $p = 0.011$, (E) NS using by one-way ANOVA, followed by Tukey post hoc test.

Fig 4. HPL-2 defective in binding H3K9me2/3 represses transcription, forms foci and supports cell identity commitment. (**A**) Schematic of the HPL-2 aromatic cage (F19, W41, F43) [11,59], and the *hpl-2(FFAA)* double point mutation, which eliminates two of the three aromatic side chains for me-lysine binding. (**B**) Representative live images of HPL-2::mKate2::3xFLAG in WT or *hpl-2(FFAA)* embryos. Scale bar, 5 µm. N = 3, n = 30. Quantification of HPL-2::mKate2 foci (**C**) number and (**D**) size from data in (**B**). N = 3. *P-values (*hpl-2(FFAA)* vs *hpl-2-WT*): (C) $p = 2.8 \times 10^{-3}$, (D) $p = 2.8 \times 10^{-3}$ by one-way ANOVA, followed by Tukey post hoc test. (**E**) gene heat map and (**F**) RNAseq scatterplot comparing gene expression between *hpl-2Δ* and *hpl-2(FFAA)* mutant embryos. N = 3, FC > 2, FDR < 0.05 (**G**) Representative DIC live images and quantification of multivulva (Muv) defects in worms expressing

hpl-2-WT, *hpl-2Δ* or *hpl-2(FFAA)* in the sensitized *lin-15A(n767)* background. Normal vulvae = circle, multivulva defects = arrowheads. N = 3. n: WT = 1437, *hpl-2Δ* = 1975, *hpl-2(FFAA)* = 1483. (**H**) Representative live image maximum projections and signal quantification of endogenously-tagged PGL-1::GFP in the heads of L4 animals. Body is outlined in dashed line; mouth is to the right. Arrowhead = faint ectopic expression. Scale bar = 10 µm, N = 3, n = 30. *p < 10^{-5}, ns = not significant by one-way ANOVA, followed by Tukey post hoc test. KS-test statistics reported in Table S4.

Fig S4. H3K9me recognition is not required for HPL-2 stability, foci targeting, or gene repression. (**A**) Representative Western blot of H3K9me peptide in vitro binding assay. Mean +/- standard error ratio of FFAA / WT bands for each peptide is shown above the blot. N = 3. *p = 1.8 x 10^{-4}, **p = 2.6 x 10^{-4} by two-sided T test. (**B**) Representative western blot of HPL-2::mKate2::3xFLAG in *hpl-2-WT* vs. *hpl-2(FFAA)* protein levels. N = 4. (**C**) Image quantification in *hpl-2-WT* vs. *hpl-2(FFAA)* of HPL-2::mKate2::3xFLAG nuclear intensity from Fig. 2D, not significant by one-way ANOVA, followed by Tukey post hoc test. (**D**) foci intensity, and (**E**) distance to the nuclear periphery as in Fig. 3E. P-values (*hpl-2(FFAA)* vs *hpl-2-WT*): (D) not significant, (E) p = 0.039 by one-way ANOVA, followed by Tukey post hoc test. (**F**) Representative images of MET-2::mNeonGreen co-expressed with HPL-2::mKate2 in WT, *met-2(catD)*, and *hpl-2(FFAA)* backgrounds. Scale bar, 5 µm. N = 3, n = 30. (**G**) Venn diagram showing overlap of *hpl-2Δ* and *hpl-2(FFAA)*-derepressed genes measured by RNAseq. N = 3, FC > 2, FDR < 0.05 Image quantification in *hpl-2-WT* vs. *hpl-2(FFAA)* of HPL-2::mKate2::3xFLAG

Fig. 5 MET-2 lacking catalytic activity supports vulva specification and germline gene repression, but requires LIN-65

(**A**) Representative DIC live images and quantification of multivulva (Muv) defects in worms expressing *met-2-WT*, *met-2Δ* or *met-2(catD)* in the sensitized *lin-15A(n767)* background. Normal vulvae = circle, multivulva defects = arrowheads. N = 3. n: WT = 1463, *met-2Δ* = 1141, *met-2(catD)* = 1346. (**B**) Representative live image maximum projections and signal quantification of endogenously-tagged PGL-1::GFP in the heads of L4 animals. Body is outlined in dashed line; mouth is to the right. Arrowhead = faint ectopic expression. Scale bar = 10 µm, N = 3, n = 30. *p < 10^{-5}, ns = not significant by one-way ANOVA, followed by Tukey post hoc test. KS-test statistics reported in Table S4. (**C**) Representative live images of endogenously tagged LIN-65::GFP in WT, *met-2Δ*, and *met-2(catD)* embryos. Scale bar, 5 µm. N = 3, n = 45. Dashed lines indicate embryo circumference. (**D**) Quantification of foci number from (C). n.d. = not detected, *met-2(catD)* vs WT p = 0.028 using two-sided Wilcoxon signed-rank test. (**E**) Quantification of Muv defects in *lin-65Δ* or *arle-14Δ* mutants in the sensitized *lin-15A(n767)* background. N = 3. n: *lin-15A* = 1159, *lin-65Δ;lin-15A* = 1199, *arle-14Δ;lin-15A* = 903. (**F**) Quantification of Muv defects in worms expressing an endogenously tagged nuclear localized NLS::met-2 in the presence or absence of *lin-65* and *lin-15A*. N = 3. n: WT = 429, *lin-15A* = 404, *lin-65Δ* = 434, *NLS::met-2*

= 548, *lin-65Δ;NLS::met-2* = 467, *lin-65Δ;lin-15A* = 650, *NLS::met-2;lin-15A* = 589, *lin-65Δ;NLS::met-2;lin-15A* = 692 . (**G**) Progeny number per worm 25°C in WT, *lin-65Δ*, NLS::met-2, and *lin-65Δ;NLS::met-2*. *N* = 3, n = 45 egg focal sections. *$p < 10^{-5}$, ns = not significant by one-way ANOVA, followed by Tukey post hoc test.

Fig. 6. HPL-2 CSD binds LIN-13 to promote focus formation and support vulva cell fate restriction. (**A**) Representative images of embryos co-expressing MET-2::mNeonGreen with HPL-2::mKate2 treated with the indicated RNAi or empty vector control. Scale bar, 5 µm. N = 3, n = 30. (**B**) anti-FLAG immunoprecipitation coupled to mass spectrometry enrichment of mKate2 and LIN-13 in untagged and HPL-2::mKate2::3xFLAG embryos. N = 3. (**C**) Schematic of chromodomain (ΔCD) or chromoshadow domain (ΔCSD) deletions created in HPL-2::mKate2 expressing animals (WT or FFAA, respectively). Positions of first and last amino acids of the deletions, replaced with Gly-Ser-Gly, are indicated. For clarity, only the short isoform is shown. (**D**) LIN-13 spectral intensity normalized to that of mKate2 in WT, *hpl-2(ΔCD)*, and *hpl-2(FFAA)ΔCSD*. N = 3. *$p = 4 \times 10^{-6}$, ns = not significant by two-sided T test. (**E**) Representative live images of HPL-2::mKate2 in WT, HPL-2-ΔCD, and HPL-2(FFAA-ΔCSD) embryos. Scale bar, 5 µm. N = 3, n = 30. (**F**) Quantification of foci intensity relative to nuclear signal from (E). HPL-2ΔCD vs WT not significant, HPL-2(FFAA-ΔCSD) vs WT $p < 2.2 \times 10^{-16}$ using two-sided Wilcoxon signed-rank test. (**G**) Quantification of Muv defects in worms expressing, *hpl-2Δ* or mKate2-tagged strains in the sensitized *lin-15A(n767)* background. N = 3. n: *hpl-2Δ* = 859, WT = 899, *hpl-2(ΔCD)* = 887, *hpl-2(FFAA)ΔCSD* = 941. (**H**) qRT-PCR of a subset of *hpl-2Δ* up-regulated genes or the control gene *lmn-1* in *hpl-2Δ* or mKate2-tagged strains. Bars show means while dots indicate individual measurements. N = 3.

Figure 7. HPL-2-LIN13 and MET-2-LIN-65 complexes act independently of each other and of H3K9me to restrict cell fate decisions

A schematic representation showing how independent interactions of the H3K9me reader (HPL-2) and writer (MET-2) with large multivalent cofactors are necessary for H3K9me-independent functions of HPL-2 and MET-2 during development. CSD-dependent interaction of HPL-2 with LIN-13 recruits HPL-2 into foci and suffices to restrict cell fate and repress transcription while MET-2 catalytic and non-catalytic activities require the intrinsically disordered domain protein LIN-65. LIN-65 is also necessary for MET-2 foci, which colocalize with HPL-2 foci. These mechanisms complement H3K9me-dependent pathways repressing genes and repetitive elements.

References

1. Nicetto, D., and Zaret, K.S. (2019). Role of H3K9me3 heterochromatin in cell identity establishment and maintenance. Curr Opin Genet Dev *55*, 1-10. 10.1016/j.gde.2019.04.013.
2. Sawh, A.N., and Mango, S.E. (2022). Chromosome organization in 4D: insights from C. elegans development. Curr Opin Genet Dev *75*, 101939. 10.1016/j.gde.2022.101939.
3. Grewal, S.I.S. (2023). The molecular basis of heterochromatin assembly and epigenetic inheritance. Mol Cell *83*, 1767-1785. 10.1016/j.molcel.2023.04.020.
4. Allshire, R.C., and Madhani, H.D. (2018). Ten principles of heterochromatin formation and function. Nat Rev Mol Cell Biol *19*, 229-244. 10.1038/nrm.2017.119.
5. Janssen, A., Colmenares, S.U., and Karpen, G.H. (2018). Heterochromatin: Guardian of the Genome. Annu Rev Cell Dev Biol *34*, 265-288. 10.1146/annurev-cellbio-100617-062653.
6. Bannister, A.J., Zegerman, P., Partridge, J.F., Miska, E.A., Thomas, J.O., Allshire, R.C., and Kouzarides, T. (2001). Selective recognition of methylated lysine 9 on histone H3 by the HP1 chromo domain. Nature *410*, 120-124. 10.1038/35065138.
7. Jacobs, S.A., and Khorasanizadeh, S. (2002). Structure of HP1 chromodomain bound to a lysine 9-methylated histone H3 tail. Science *295*, 2080-2083. 10.1126/science.1069473.
8. Nielsen, P.R., Nietlispach, D., Mott, H.R., Callaghan, J., Bannister, A., Kouzarides, T., Murzin, A.G., Murzina, N.V., and Laue, E.D. (2002). Structure of the HP1 chromodomain bound to histone H3 methylated at lysine 9. Nature *416*, 103-107. 10.1038/nature722.
9. Kumar, A., and Kono, H. (2020). Heterochromatin protein 1 (HP1): interactions with itself and chromatin components. Biophys Rev *12*, 387-400. 10.1007/s12551-020-00663-y.
10. Mendez, D.L., Mandt, R.E., and Elgin, S.C. (2013). Heterochromatin Protein 1a (HP1a) partner specificity is determined by critical amino acids in the chromo shadow domain and C-terminal extension. J Biol Chem *288*, 22315-22323. 10.1074/jbc.M113.468413.
11. Thiru, A., Nietlispach, D., Mott, H.R., Okuwaki, M., Lyon, D., Nielsen, P.R., Hirshberg, M., Verreault, A., Murzina, N.V., and Laue, E.D. (2004). Structural basis of HP1/PXVXL motif peptide interactions and HP1 localisation to heterochromatin. EMBO J *23*, 489-499. 10.1038/sj.emboj.7600088.
12. Eissenberg, J.C., and Elgin, S.C. (2014). HP1a: a structural chromosomal protein regulating transcription. Trends Genet *30*, 103-110. 10.1016/j.tig.2014.01.002.
13. Lou, J., Deng, Q., Zhang, X., Bell, C.C., Das, A.B., Bediaga, N.G., Zlatic, C.O., Johanson, T.M., Allan, R.S., Griffin, M.D.W., et al. (2024). Heterochromatin protein 1 alpha (HP1alpha) undergoes a monomer to dimer transition that opens and compacts live cell genome architecture. Nucleic Acids Res *52*, 10918-10933. 10.1093/nar/gkae720.
14. Collombet, S., Rall, I., Dugast-Darzacq, C., Heckert, A., Halavatyi, A., Le Saux, A., Dailey, G., Darzacq, X., and Heard, E. (2023). RNA polymerase II depletion from the inactive X chromosome territory is not mediated by physical compartmentalization. Nat Struct Mol Biol *30*, 1216-1223. 10.1038/s41594-023-01008-5.
15. Methot, S.P., Padeken, J., Brancati, G., Zeller, P., Delaney, C.E., Gaidatzis, D., Kohler, H., van Oudenaarden, A., Grosshans, H., and Gasser, S.M. (2021). H3K9me selectively blocks transcription factor activity and ensures differentiated tissue integrity. Nature cell biology *23*, 1163-1175. 10.1038/s41556-021-00776-w.
16. Schotta, G., Ebert, A., Krauss, V., Fischer, A., Hoffmann, J., Rea, S., Jenuwein, T., Dorn, R., and Reuter, G. (2002). Central role of Drosophila SU(VAR)3-9 in histone H3-K9 methylation and heterochromatic gene silencing. EMBO J *21*, 1121-1131. 10.1093/emboj/21.5.1121.
17. Wang, T., Xu, C., Liu, Y., Fan, K., Li, Z., Sun, X., Ouyang, H., Zhang, X., Zhang, J., Li, Y., et al. (2012). Crystal structure of the human SUV39H1 chromodomain and its recognition of histone H3K9me2/3. PLoS One *7*, e52977. 10.1371/journal.pone.0052977.
18. Padeken, J., Methot, S.P., and Gasser, S.M. (2022). Establishment of H3K9-methylated heterochromatin and its functions in tissue differentiation and maintenance. Nat Rev Mol Cell Biol *23*, 623-640. 10.1038/s41580-022-00483-w.

19. Nicetto, D., Donahue, G., Jain, T., Peng, T., Sidoli, S., Sheng, L., Montavon, T., Becker, J.S., Grindheim, J.M., Blahnik, K., et al. (2019). H3K9me3-heterochromatin loss at protein-coding genes enables developmental lineage specification. Science *363*, 294-297. 10.1126/science.aau0583.
20. Chen, M.W., Hua, K.T., Kao, H.J., Chi, C.C., Wei, L.H., Johansson, G., Shiah, S.G., Chen, P.S., Jeng, Y.M., Cheng, T.Y., et al. (2010). H3K9 histone methyltransferase G9a promotes lung cancer invasion and metastasis by silencing the cell adhesion molecule Ep-CAM. Cancer Res *70*, 7830-7840. 10.1158/0008-5472.CAN-10-0833.
21. Griffin, G.K., Wu, J., Iracheta-Vellve, A., Patti, J.C., Hsu, J., Davis, T., Dele-Oni, D., Du, P.P., Halawi, A.G., Ishizuka, J.J., et al. (2021). Epigenetic silencing by SETDB1 suppresses tumour intrinsic immunogenicity. Nature *595*, 309-314. 10.1038/s41586-021-03520-4.
22. Karanth, A.V., Maniswami, R.R., Prashanth, S., Govindaraj, H., Padmavathy, R., Jegatheesan, S.K., Mullangi, R., and Rajagopal, S. (2017). Emerging role of SETDB1 as a therapeutic target. Expert Opin Ther Targets *21*, 319-331. 10.1080/14728222.2017.1279604.
23. Prashanth, S., Radha Maniswami, R., Rajajeyabalachandran, G., and Jegatheesan, S.K. (2024). SETDB1, an H3K9-specific methyltransferase: An attractive epigenetic target to combat cancer. Drug Discov Today *29*, 103982. 10.1016/j.drudis.2024.103982.
24. Zhang, W., Li, J., Suzuki, K., Qu, J., Wang, P., Zhou, J., Liu, X., Ren, R., Xu, X., Ocampo, A., et al. (2015). Aging stem cells. A Werner syndrome stem cell model unveils heterochromatin alterations as a driver of human aging. Science *348*, 1160-1163. 10.1126/science.aaa1356.
25. Zeller, P., Padeken, J., van Schendel, R., Kalck, V., Tijsterman, M., and Gasser, S.M. (2016). Histone H3K9 methylation is dispensable for Caenorhabditis elegans development but suppresses RNA:DNA hybrid-associated repeat instability. Nat Genet *48*, 1385-1395. 10.1038/ng.3672.
26. Lee, T.W., David, H.S., Engstrom, A.K., Carpenter, B.S., and Katz, D.J. (2019). Repressive H3K9me2 protects lifespan against the transgenerational burden of COMPASS activity in C. elegans. Elife *8*. 10.7554/eLife.48498.
27. Mutlu, B., Chen, H.M., Gutnik, S., Hall, D.H., Keppler-Ross, S., and Mango, S.E. (2019). Distinct functions and temporal regulation of methylated histone H3 during early embryogenesis. Development *146*. 10.1242/dev.174516.
28. Mutlu, B., Chen, H.M., Moresco, J.J., Orelo, B.D., Yang, B., Gaspar, J.M., Keppler-Ross, S., Yates, J.R., 3rd, Hall, D.H., Maine, E.M., and Mango, S.E. (2018). Regulated nuclear accumulation of a histone methyltransferase times the onset of heterochromatin formation in C. elegans embryos. Sci Adv *4*, eaat6224. 10.1126/sciadv.aat6224.
29. McMurchy, A.N., Stempor, P., Gaarenstroom, T., Wysolmerski, B., Dong, Y., Aussianikava, D., Appert, A., Huang, N., Kolasinska-Zwierz, P., Sapetschnig, A., et al. (2017). A team of heterochromatin factors collaborates with small RNA pathways to combat repetitive elements and germline stress. Elife *6*. 10.7554/eLife.21666.
30. Meister, P., Mango, S.E., and Gasser, S.M. (2011). Locking the genome: nuclear organization and cell fate. Curr Opin Genet Dev *21*, 167-174. 10.1016/j.gde.2011.01.023.
31. Kaaij, L.J.T., Mohn, F., van der Weide, R.H., de Wit, E., and Buhler, M. (2019). The ChAHP Complex Counteracts Chromatin Looping at CTCF Sites that Emerged from SINE Expansions in Mouse. Cell *178*, 1437-1451 e1414. 10.1016/j.cell.2019.08.007.
32. Ostapcuk, V., Mohn, F., Carl, S.H., Basters, A., Hess, D., Iesmantavicius, V., Lampersberger, L., Flemr, M., Pandey, A., Thoma, N.H., et al. (2018). Activity-dependent neuroprotective protein recruits HP1 and CHD4 to control lineage-specifying genes. Nature *557*, 739-743. 10.1038/s41586-018-0153-8.
33. Biswas, S., Chen, Z., Karslake, J.D., Farhat, A., Ames, A., Raiymbek, G., Freddolino, P.L., Biteen, J.S., and Ragunathan, K. (2022). HP1 oligomerization compensates for low-affinity H3K9me recognition and provides a tunable mechanism for heterochromatin-specific localization. Sci Adv *8*, eabk0793. 10.1126/sciadv.abk0793.

34. Figueiredo, M.L., Philip, P., Stenberg, P., and Larsson, J. (2012). HP1a recruitment to promoters is independent of H3K9 methylation in Drosophila melanogaster. PLoS Genet *8*, e1003061. 10.1371/journal.pgen.1003061.
35. Smothers, J.F., and Henikoff, S. (2001). The hinge and chromo shadow domain impart distinct targeting of HP1-like proteins. Mol Cell Biol *21*, 2555-2569. 10.1128/MCB.21.7.2555-2569.2001.
36. Zhao, T., Heyduk, T., and Eissenberg, J.C. (2001). Phosphorylation site mutations in heterochromatin protein 1 (HP1) reduce or eliminate silencing activity. J Biol Chem *276*, 9512-9518. 10.1074/jbc.M010098200.
37. Erdel, F., Rademacher, A., Vlijm, R., Tunnermann, J., Frank, L., Weinmann, R., Schweigert, E., Yserentant, K., Hummert, J., Bauer, C., et al. (2020). Mouse Heterochromatin Adopts Digital Compaction States without Showing Hallmarks of HP1-Driven Liquid-Liquid Phase Separation. Mol Cell *78*, 236-249 e237. 10.1016/j.molcel.2020.02.005.
38. Larson, A.G., Elnatan, D., Keenen, M.M., Trnka, M.J., Johnston, J.B., Burlingame, A.L., Agard, D.A., Redding, S., and Narlikar, G.J. (2017). Liquid droplet formation by HP1alpha suggests a role for phase separation in heterochromatin. Nature *547*, 236-240. 10.1038/nature22822.
39. Strom, A.R., Eeftens, J.M., Polyachenko, Y., Weaver, C.J., Watanabe, H.F., Bracha, D., Orlovsky, N.D., Jumper, C.C., Jacobs, W.M., and Brangwynne, C.P. (2024). Interplay of condensation and chromatin binding underlies BRD4 targeting. Mol Biol Cell *35*, ar88. 10.1091/mbc.E24-01-0046.
40. Harr, J.C., Gonzalez-Sandoval, A., and Gasser, S.M. (2016). Histones and histone modifications in perinuclear chromatin anchoring: from yeast to man. EMBO Rep *17*, 139-155. 10.15252/embr.201541809.
41. Delaney, C.E., Methot, S.P., Guidi, M., Katic, I., Gasser, S.M., and Padeken, J. (2019). Heterochromatic foci and transcriptional repression by an unstructured MET-2/SETDB1 co-factor LIN-65. J Cell Biol *218*, 820-838. 10.1083/jcb.201811038.
42. Garrigues, J.M., Sidoli, S., Garcia, B.A., and Strome, S. (2015). Defining heterochromatin in C. elegans through genome-wide analysis of the heterochromatin protein 1 homolog HPL-2. Genome Res *25*, 76-88. 10.1101/gr.180489.114.
43. Meister, P., Schott, S., Bedet, C., Xiao, Y., Rohner, S., Bodennec, S., Hudry, B., Molin, L., Solari, F., Gasser, S.M., and Palladino, F. (2011). Caenorhabditis elegans Heterochromatin protein 1 (HPL-2) links developmental plasticity, longevity and lipid metabolism. Genome Biol *12*, R123. 10.1186/gb-2011-12-12-r123.
44. Padeken, J., Zeller, P., Towbin, B., Katic, I., Kalck, V., Methot, S.P., and Gasser, S.M. (2019). Synergistic lethality between BRCA1 and H3K9me2 loss reflects satellite derepression. Genes Dev *33*, 436-451. 10.1101/gad.322495.118.
45. Andersen, E.C., and Horvitz, H.R. (2007). Two C. elegans histone methyltransferases repress lin-3 EGF transcription to inhibit vulval development. Development *134*, 2991-2999. 10.1242/dev.009373.
46. Simonet, T., Dulermo, R., Schott, S., and Palladino, F. (2007). Antagonistic functions of SET-2/SET1 and HPL/HP1 proteins in C. elegans development. Dev Biol *312*, 367-383. 10.1016/j.ydbio.2007.09.035.
47. Poulin, G., Dong, Y., Fraser, A.G., Hopper, N.A., and Ahringer, J. (2005). Chromatin regulation and sumoylation in the inhibition of Ras-induced vulval development in Caenorhabditis elegans. EMBO J *24*, 2613-2623. 10.1038/sj.emboj.7600726.
48. Delaney, C.E., Methot, S.P., Kalck, V., Seebacher, J., Hess, D., Gasser, S.M., and Padeken, J. (2022). SETDB1-like MET-2 promotes transcriptional silencing and development independently of its H3K9me-associated catalytic activity. Nat Struct Mol Biol *29*, 85-96. 10.1038/s41594-021-00712-4.
49. Tsusaka, T., Shimura, C., and Shinkai, Y. (2019). ATF7IP regulates SETDB1 nuclear localization and increases its ubiquitination. EMBO Rep *20*, e48297. 10.15252/embr.201948297.

50. Coustham, V., Bedet, C., Monier, K., Schott, S., Karali, M., and Palladino, F. (2006). The C. elegans HP1 homologue HPL-2 and the LIN-13 zinc finger protein form a complex implicated in vulval development. Dev Biol *297*, 308-322. 10.1016/j.ydbio.2006.04.474.
51. Couteau, F., Guerry, F., Muller, F., and Palladino, F. (2002). A heterochromatin protein 1 homologue in Caenorhabditis elegans acts in germline and vulval development. EMBO Rep *3*, 235-241. 10.1093/embo-reports/kvf051.
52. Patel, T., and Hobert, O. (2017). Coordinated control of terminal differentiation and restriction of cellular plasticity. Elife *6*. 10.7554/eLife.24100.
53. Towbin, B.D., Gonzalez-Aguilera, C., Sack, R., Gaidatzis, D., Kalck, V., Meister, P., Askjaer, P., and Gasser, S.M. (2012). Step-wise methylation of histone H3K9 positions heterochromatin at the nuclear periphery. Cell *150*, 934-947. 10.1016/j.cell.2012.06.051.
54. Ashe, A., Sapetschnig, A., Weick, E.M., Mitchell, J., Bagijn, M.P., Cording, A.C., Doebley, A.L., Goldstein, L.D., Lehrbach, N.J., Le Pen, J., et al. (2012). piRNAs can trigger a multigenerational epigenetic memory in the germline of C. elegans. Cell *150*, 88-99. 10.1016/j.cell.2012.06.018.
55. Meister, P., Towbin, B.D., Pike, B.L., Ponti, A., and Gasser, S.M. (2010). The spatial dynamics of tissue-specific promoters during C. elegans development. Genes Dev *24*, 766-782. 10.1101/gad.559610.
56. Ferguson, E.L., and Horvitz, H.R. (1989). The multivulva phenotype of certain Caenorhabditis elegans mutants results from defects in two functionally redundant pathways. Genetics *123*, 109-121. 10.1093/genetics/123.1.109.
57. Padeken, J., Methot, S., Zeller, P., Delaney, C.E., Kalck, V., and Gasser, S.M. (2021). Argonaute NRDE-3 and MBT domain protein LIN-61 redundantly recruit an H3K9me3 HMT to prevent embryonic lethality and transposon expression. Genes Dev *35*, 82-101. 10.1101/gad.344234.120.
58. Gonzalez-Sandoval, A., Towbin, B.D., Kalck, V., Cabianca, D.S., Gaidatzis, D., Hauer, M.H., Geng, L., Wang, L., Yang, T., Wang, X., et al. (2015). Perinuclear Anchoring of H3K9-Methylated Chromatin Stabilizes Induced Cell Fate in C. elegans Embryos. Cell *163*, 1333-1347. 10.1016/j.cell.2015.10.066.
59. Beaver, J.E., and Waters, M.L. (2016). Molecular Recognition of Lys and Arg Methylation. ACS Chem Biol *11*, 643-653. 10.1021/acschembio.5b00996.
60. Zhebrun, A., Ni, J.Z., Corveleyn, L., Ghosh Roy, S., Sidoli, S., and Gu, S.G. (2025). Two H3K23 histone methyltransferases, SET-32 and SET-21, function synergistically to promote nuclear RNAi-mediated transgenerational epigenetic inheritance in Caenorhabditis elegans. Genetics *229*. 10.1093/genetics/iyae206.
61. Knutson, A.K., Rechtsteiner, A., and Strome, S. (2016). Reevaluation of whether a soma-to-germ-line transformation extends lifespan in Caenorhabditis elegans. Proc Natl Acad Sci U S A *113*, 3591-3596. 10.1073/pnas.1523402113.
62. Petrella, L.N., Wang, W., Spike, C.A., Rechtsteiner, A., Reinke, V., and Strome, S. (2011). synMuv B proteins antagonize germline fate in the intestine and ensure C. elegans survival. Development *138*, 1069-1079. 10.1242/dev.059501.
63. Saffer, A.M., Kim, D.H., van Oudenaarden, A., and Horvitz, H.R. (2011). The Caenorhabditis elegans synthetic multivulva genes prevent ras pathway activation by tightly repressing global ectopic expression of lin-3 EGF. PLoS Genet *7*, e1002418. 10.1371/journal.pgen.1002418.
64. Wu, X., Shi, Z., Cui, M., Han, M., and Ruvkun, G. (2012). Repression of germline RNAi pathways in somatic cells by retinoblastoma pathway chromatin complexes. PLoS Genet *8*, e1002542. 10.1371/journal.pgen.1002542.
65. Putnam, A., Cassani, M., Smith, J., and Seydoux, G. (2019). A gel phase promotes condensation of liquid P granules in Caenorhabditis elegans embryos. Nat Struct Mol Biol *26*, 220-226. 10.1038/s41594-019-0193-2.
66. Swenson, J.M., Colmenares, S.U., Strom, A.R., Costes, S.V., and Karpen, G.H. (2016). The composition and organization of Drosophila heterochromatin are heterogeneous and dynamic. Elife *5*. 10.7554/eLife.16096.

67. Ceol, C.J., Stegmeier, F., Harrison, M.M., and Horvitz, H.R. (2006). Identification and classification of genes that act antagonistically to let-60 Ras signaling in Caenorhabditis elegans vulval development. Genetics *173*, 709-726. 10.1534/genetics.106.056465.
68. Maharana, S., Wang, J., Papadopoulos, D.K., Richter, D., Pozniakovsky, A., Poser, I., Bickle, M., Rizk, S., Guillen-Boixet, J., Franzmann, T.M., et al. (2018). RNA buffers the phase separation behavior of prion-like RNA binding proteins. Science *360*, 918-921. 10.1126/science.aar7366.
69. Mohanty, P., Kapoor, U., Sundaravadivelu Devarajan, D., Phan, T.M., Rizuan, A., and Mittal, J. (2022). Principles Governing the Phase Separation of Multidomain Proteins. Biochemistry *61*, 2443-2455. 10.1021/acs.biochem.2c00210.
70. Melendez, A., and Greenwald, I. (2000). Caenorhabditis elegans lin-13, a member of the LIN-35 Rb class of genes involved in vulval development, encodes a protein with zinc fingers and an LXCXE motif. Genetics *155*, 1127-1137. 10.1093/genetics/155.3.1127.
71. Thomas, J.H., Ceol, C.J., Schwartz, H.T., and Horvitz, H.R. (2003). New genes that interact with lin-35 Rb to negatively regulate the let-60 ras pathway in Caenorhabditis elegans. Genetics *164*, 135-151. 10.1093/genetics/164.1.135.
72. Canzio, D., Larson, A., and Narlikar, G.J. (2014). Mechanisms of functional promiscuity by HP1 proteins. Trends Cell Biol *24*, 377-386. 10.1016/j.tcb.2014.01.002.
73. Jenuwein, T., and Allis, C.D. (2001). Translating the histone code. Science *293*, 1074-1080. 10.1126/science.1063127.
74. Bulut-Karslioglu, A., De La Rosa-Velazquez, I.A., Ramirez, F., Barenboim, M., Onishi-Seebacher, M., Arand, J., Galan, C., Winter, G.E., Engist, B., Gerle, B., et al. (2014). Suv39h-dependent H3K9me3 marks intact retrotransposons and silences LINE elements in mouse embryonic stem cells. Mol Cell *55*, 277-290. 10.1016/j.molcel.2014.05.029.
75. Peng, J.C., and Karpen, G.H. (2007). H3K9 methylation and RNA interference regulate nucleolar organization and repeated DNA stability. Nature cell biology *9*, 25-35. 10.1038/ncb1514.
76. Peters, A.H., O'Carroll, D., Scherthan, H., Mechtler, K., Sauer, S., Schofer, C., Weipoltshammer, K., Pagani, M., Lachner, M., Kohlmaier, A., et al. (2001). Loss of the Suv39h histone methyltransferases impairs mammalian heterochromatin and genome stability. Cell *107*, 323-337.
77. Probst, A.V., Okamoto, I., Casanova, M., El Marjou, F., Le Baccon, P., and Almouzni, G. (2010). A strand-specific burst in transcription of pericentric satellites is required for chromocenter formation and early mouse development. Dev Cell *19*, 625-638. 10.1016/j.devcel.2010.09.002.
78. Penke, T.J., McKay, D.J., Strahl, B.D., Matera, A.G., and Duronio, R.J. (2016). Direct interrogation of the role of H3K9 in metazoan heterochromatin function. Genes Dev *30*, 1866-1880. 10.1101/gad.286278.116.
79. Ciabrelli, F., Rabbani, L., Cardamone, F., Zenk, F., Loser, E., Schachtle, M.A., Mazina, M., Loubiere, V., and Iovino, N. (2023). CBP and Gcn5 drive zygotic genome activation independently of their catalytic activity. Sci Adv *9*, eadf2687. 10.1126/sciadv.adf2687.
80. Ferrie, J.J., Karr, J.P., Graham, T.G.W., Dailey, G.M., Zhang, G., Tjian, R., and Darzacq, X. (2024). p300 is an obligate integrator of combinatorial transcription factor inputs. Mol Cell *84*, 234-243 e234. 10.1016/j.molcel.2023.12.004.
81. Hunt, G., Boija, A., and Mannervik, M. (2022). p300/CBP sustains Polycomb silencing by non-enzymatic functions. Mol Cell *82*, 3580-3597 e3589. 10.1016/j.molcel.2022.09.005.
82. Dorighi, K.M., Swigut, T., Henriques, T., Bhanu, N.V., Scruggs, B.S., Nady, N., Still, C.D., 2nd, Garcia, B.A., Adelman, K., and Wysocka, J. (2017). Mll3 and Mll4 Facilitate Enhancer RNA Synthesis and Transcription from Promoters Independently of H3K4 Monomethylation. Mol Cell *66*, 568-576 e564. 10.1016/j.molcel.2017.04.018.
83. Jiang, Q., Ang, J.Y.J., Lee, A.Y., Cao, Q., Li, K.Y., Yip, K.Y., and Leung, D.C.Y. (2020). G9a Plays Distinct Roles in Maintaining DNA Methylation, Retrotransposon Silencing, and Chromatin Looping. Cell Rep *33*, 108315. 10.1016/j.celrep.2020.108315.

84. Tachibana, M., Matsumura, Y., Fukuda, M., Kimura, H., and Shinkai, Y. (2008). G9a/GLP complexes independently mediate H3K9 and DNA methylation to silence transcription. EMBO J *27*, 2681-2690. 10.1038/emboj.2008.192.
85. Dong, L., Liao, H., Zhao, L., Wang, J., Wang, C., Wang, B., Sun, Y., Xu, L., Xia, Y., Ling, S., et al. (2023). A functional crosstalk between the H3K9 methylation writers and their reader HP1 in safeguarding embryonic stem cell identity. Stem Cell Reports *18*, 1775-1792. 10.1016/j.stemcr.2023.08.004.
86. Atinbayeva, N., Valent, I., Zenk, F., Loeser, E., Rauer, M., Herur, S., Quarato, P., Pyrowolakis, G., Gomez-Auli, A., Mittler, G., et al. (2024). Inheritance of H3K9 methylation regulates genome architecture in Drosophila early embryos. EMBO J *43*, 2685-2714. 10.1038/s44318-024-00127-z.
87. Nakao, M., Sato, Y., Aizawa, A., and Kimura, H. (2024). Mode of SUV420H2 heterochromatin localization through multiple HP1 binding motifs in the heterochromatic targeting module. Genes Cells *29*, 361-379. 10.1111/gtc.13109.
88. Schotta, G., Ebert, A., and Reuter, G. (2003). SU(VAR)3-9 is a conserved key function in heterochromatic gene silencing. Genetica *117*, 149-158. 10.1023/a:1022923508198.
89. Li, Y., Kirschmann, D.A., and Wallrath, L.L. (2002). Does heterochromatin protein 1 always follow code? Proc Natl Acad Sci U S A *99 Suppl 4*, 16462-16469. 10.1073/pnas.162371699.
90. Lupo, A., Cesaro, E., Montano, G., Zurlo, D., Izzo, P., and Costanzo, P. (2013). KRAB-Zinc Finger Proteins: A Repressor Family Displaying Multiple Biological Functions. Curr Genomics *14*, 268-278. 10.2174/1389202913149990002.
91. Murzina, N., Verreault, A., Laue, E., and Stillman, B. (1999). Heterochromatin dynamics in mouse cells: interaction between chromatin assembly factor 1 and HP1 proteins. Mol Cell *4*, 529-540. 10.1016/s1097-2765(00)80204-x.
92. Schultz, D.C., Ayyanathan, K., Negorev, D., Maul, G.G., and Rauscher, F.J., 3rd (2002). SETDB1: a novel KAP-1-associated histone H3, lysine 9-specific methyltransferase that contributes to HP1-mediated silencing of euchromatic genes by KRAB zinc-finger proteins. Genes Dev *16*, 919-932. 10.1101/gad.973302.
93. Koester-Eiserfunke, N., and Fischle, W. (2011). H3K9me2/3 binding of the MBT domain protein LIN-61 is essential for Caenorhabditis elegans vulva development. PLoS Genet *7*, e1002017. 10.1371/journal.pgen.1002017.
94. Banani, S.F., Lee, H.O., Hyman, A.A., and Rosen, M.K. (2017). Biomolecular condensates: organizers of cellular biochemistry. Nat Rev Mol Cell Biol *18*, 285-298. 10.1038/nrm.2017.7.
95. Gibson, B.A., Doolittle, L.K., Schneider, M.W.G., Jensen, L.E., Gamarra, N., Henry, L., Gerlich, D.W., Redding, S., and Rosen, M.K. (2019). Organization of Chromatin by Intrinsic and Regulated Phase Separation. Cell *179*, 470-484 e421. 10.1016/j.cell.2019.08.037.
96. Ling, Y.H., Ye, Z., Liang, C., Yu, C., Park, G., Corden, J.L., and Wu, C. (2024). Disordered C-terminal domain drives spatiotemporal confinement of RNAPII to enhance search for chromatin targets. Nature cell biology *26*, 581-592. 10.1038/s41556-024-01382-2.
97. Patil, A., Strom, A.R., Paulo, J.A., Collings, C.K., Ruff, K.M., Shinn, M.K., Sankar, A., Cervantes, K.S., Wauer, T., St Laurent, J.D., et al. (2023). A disordered region controls cBAF activity via condensation and partner recruitment. Cell *186*, 4936-4955 e4926. 10.1016/j.cell.2023.08.032.
98. Strom, A.R., Emelyanov, A.V., Mir, M., Fyodorov, D.V., Darzacq, X., and Karpen, G.H. (2017). Phase separation drives heterochromatin domain formation. Nature *547*, 241-245. 10.1038/nature22989.
99. Theunissen, O., Rudt, F., Guddat, U., Mentzel, H., and Pieler, T. (1992). RNA and DNA binding zinc fingers in Xenopus TFIIIA. Cell *71*, 679-690. 10.1016/0092-8674(92)90601-8.
100. Keller, C., Adaixo, R., Stunnenberg, R., Woolcock, K.J., Hiller, S., and Buhler, M. (2012). HP1(Swi6) mediates the recognition and destruction of heterochromatic RNA transcripts. Mol Cell *47*, 215-227. 10.1016/j.molcel.2012.05.009.

101. Koch, C.M., Honemann-Capito, M., Egger-Adam, D., and Wodarz, A. (2009). Windei, the Drosophila homolog of mAM/MCAF1, is an essential cofactor of the H3K9 methyl transferase dSETDB1/Eggless in germ line development. PLoS Genet *5*, e1000644. 10.1371/journal.pgen.1000644.
102. Osumi, K., Sato, K., Murano, K., Siomi, H., and Siomi, M.C. (2019). Essential roles of Windei and nuclear monoubiquitination of Eggless/SETDB1 in transposon silencing. EMBO Rep *20*, e48296. 10.15252/embr.201948296.
103. Timms, R.T., Tchasovnikarova, I.A., Antrobus, R., Dougan, G., and Lehner, P.J. (2016). ATF7IP-Mediated Stabilization of the Histone Methyltransferase SETDB1 Is Essential for Heterochromatin Formation by the HUSH Complex. Cell Rep *17*, 653-659. 10.1016/j.celrep.2016.09.050.
104. Kamath, R.S., Martinez-Campos, M., Zipperlen, P., Fraser, A.G., and Ahringer, J. (2001). Effectiveness of specific RNA-mediated interference through ingested double-stranded RNA in Caenorhabditis elegans. Genome Biol *2*, RESEARCH0002. 10.1186/gb-2000-2-1-research0002.
105. Timmons, L., Court, D.L., and Fire, A. (2001). Ingestion of bacterially expressed dsRNAs can produce specific and potent genetic interference in C. elegans. Gene *263*, 103-112.
106. Ghanta, K.S., and Mello, C.C. (2020). Melting dsDNA Donor Molecules Greatly Improves Precision Genome Editing in Caenorhabditis elegans. Genetics *216*, 643-650. 10.1534/genetics.120.303564.
107. Dietz, C., and Berthold, M.R. (2016). KNIME for Open-Source Bioimage Analysis: A Tutorial. Adv Anat Embryol Cell Biol *219*, 179-197. 10.1007/978-3-319-28549-8_7.
108. Raiymbek, G., An, S., Khurana, N., Gopinath, S., Larkin, A., Biswas, S., Trievel, R.C., Cho, U.S., and Ragunathan, K. (2020). An H3K9 methylation-dependent protein interaction regulates the non-enzymatic functions of a putative histone demethylase. Elife *9*. 10.7554/eLife.53155.
109. Hoogewijs, D., Houthoofd, K., Matthijssens, F., Vandesompele, J., and Vanfleteren, J.R. (2008). Selection and validation of a set of reliable reference genes for quantitative sod gene expression analysis in C. elegans. BMC Mol Biol *9*, 9. 10.1186/1471-2199-9-9.
110. Nolan, T., Hands, R.E., and Bustin, S.A. (2006). Quantification of mRNA using real-time RT-PCR. Nat Protoc *1*, 1559-1582. 10.1038/nprot.2006.236.
111. Kolberg, L., Raudvere, U., Kuzmin, I., Adler, P., Vilo, J., and Peterson, H. (2023). g:Profiler-interoperable web service for functional enrichment analysis and gene identifier mapping (2023 update). Nucleic Acids Res *51*, W207-W212. 10.1093/nar/gkad347.

Figure 01: MET-2 and HPL-2 colocalize independently in heterochromatic foci

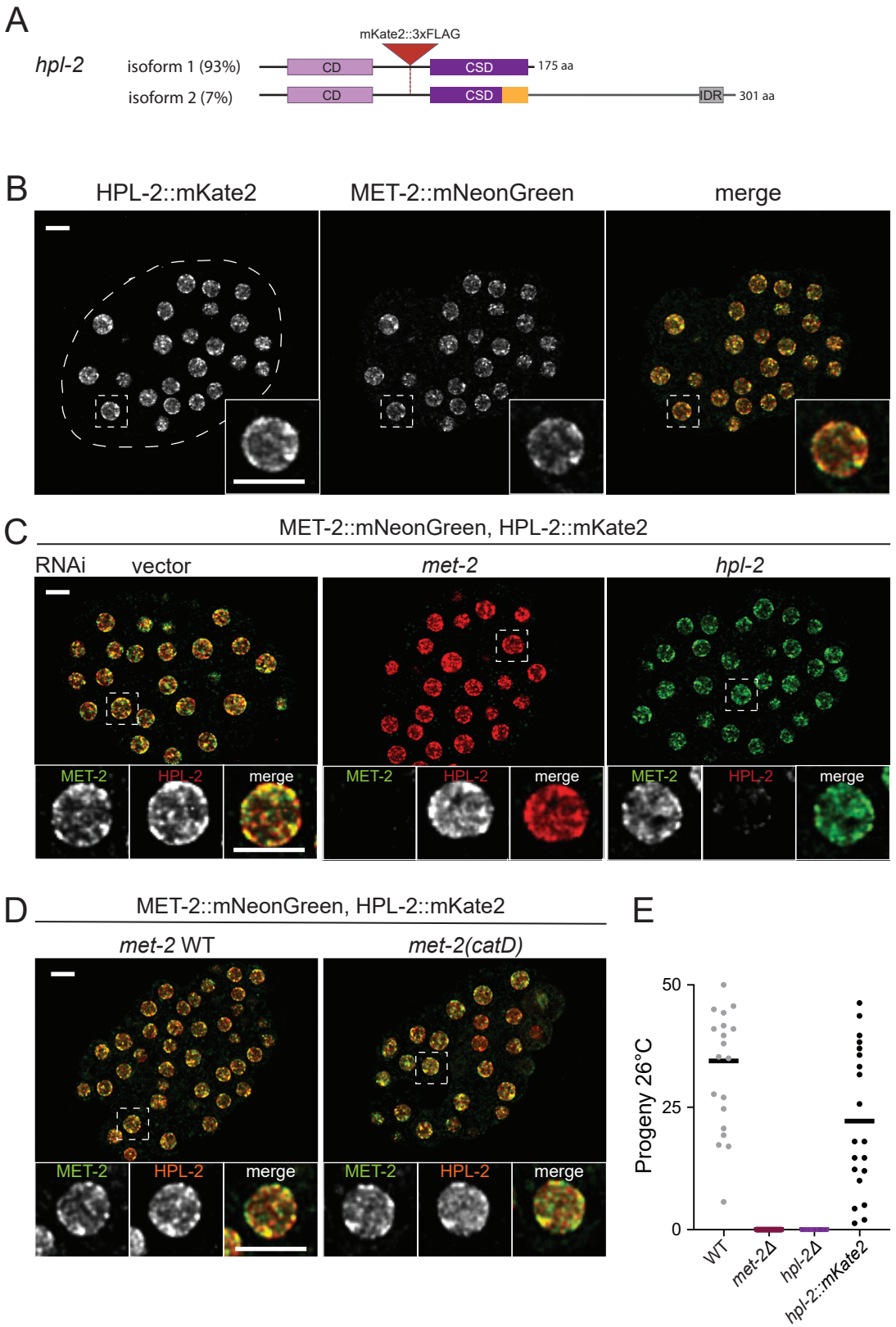

supplemental Figure S1: Other chromatin factors do not affect MET-2 and HPL-2 foci

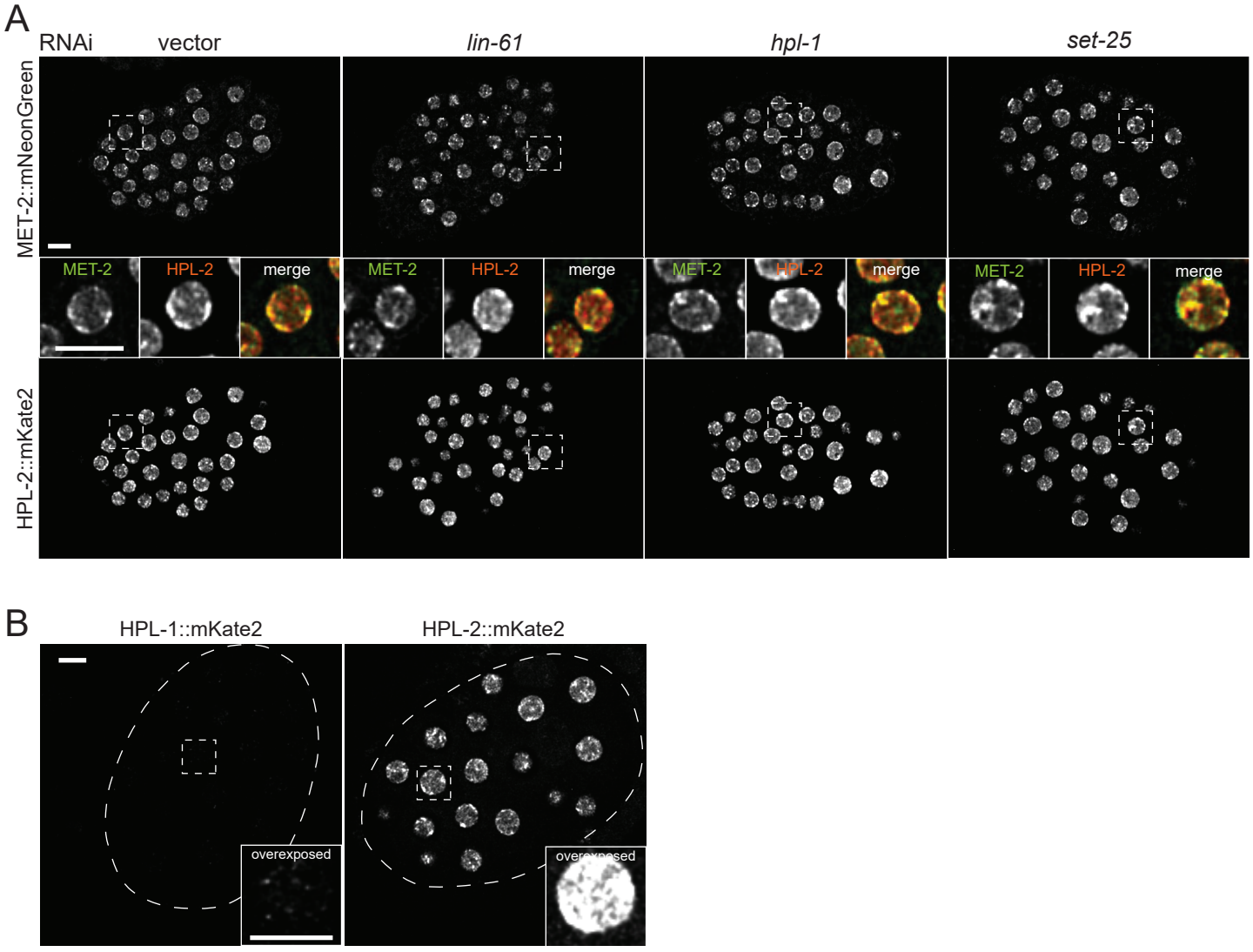

Figure 02: H3K9me and HPL-2 act independently to repress transcription

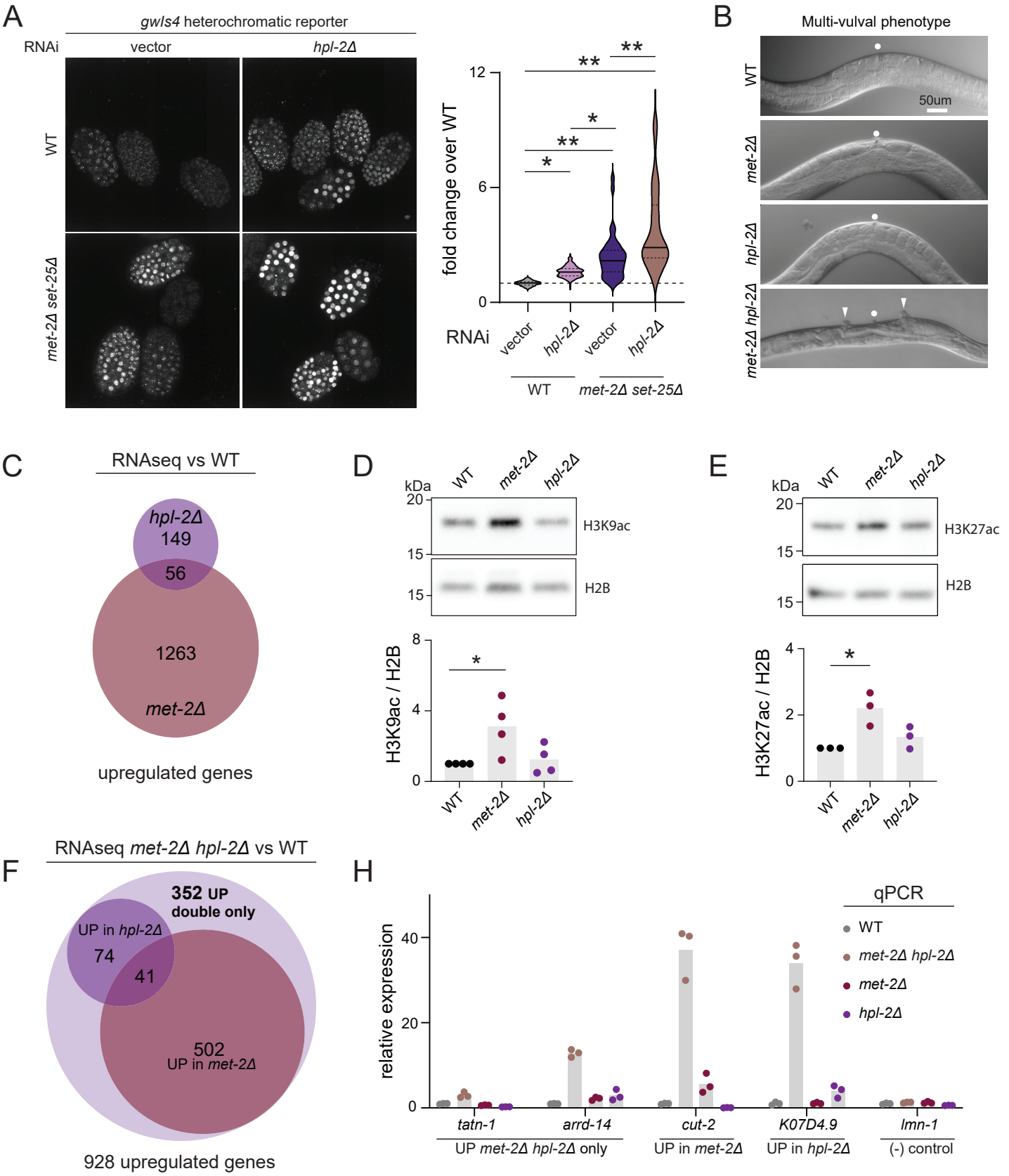

Supplemental Figure S2: SET-25 repression is similar to MET-2 repression

A

RNAseq vs WT

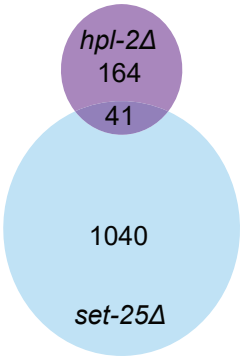

Upregulated genes

B

RNAseq vs WT

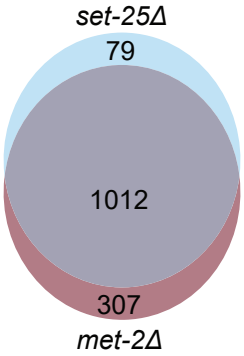

Upregulated genes

C

met-2Δ hpl-2Δ vs WT
upregulated repeat families

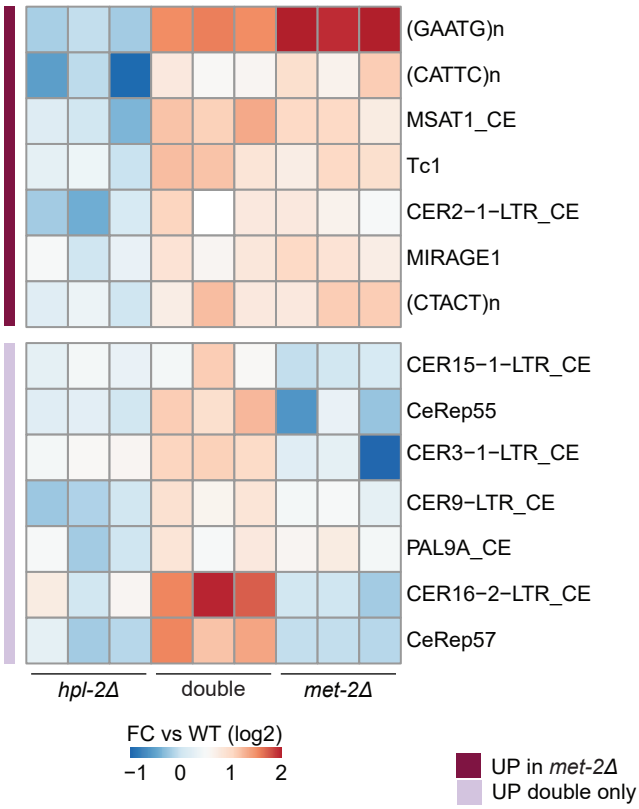

D

GO terms *met-2Δ hpl-2Δ* upregulated genes

term_id	term_name	term_size	intersection_size	p_value
GO:0042744	hydrogen peroxide catabolic process	3	2	5.1e−02
GO:0000786	nucleosome	87	7	6.6e−04
GO:0032993	protein−DNA complex	92	7	9.6e−04
GO:0000785	chromatin	120	7	5.5e−03
GO:0005694	chromosome	181	7	7.0e−02
GO:0030527	structural constituent of chromatin	85	7	3.6e−03
GO:0005198	structural molecule activity	445	14	1.9e−02
GO:0004096	catalase activity	3	2	5.7e−02
GO:0031177	phosphopantetheine binding	3	2	5.7e−02

E

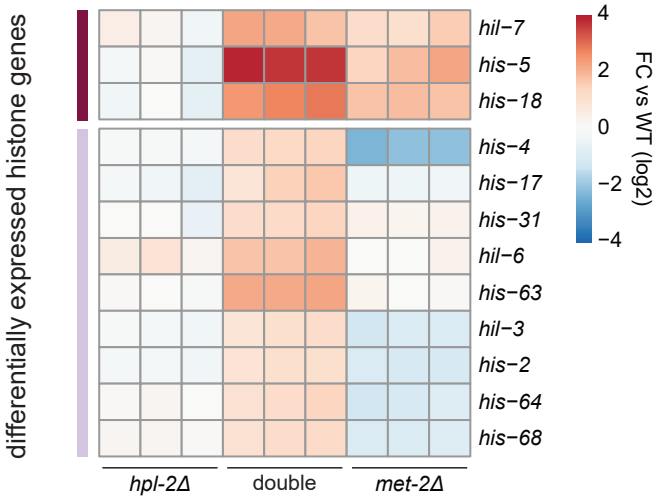

Figure 03: HPL-2 forms nuclear foci independently of H3K9 methylation

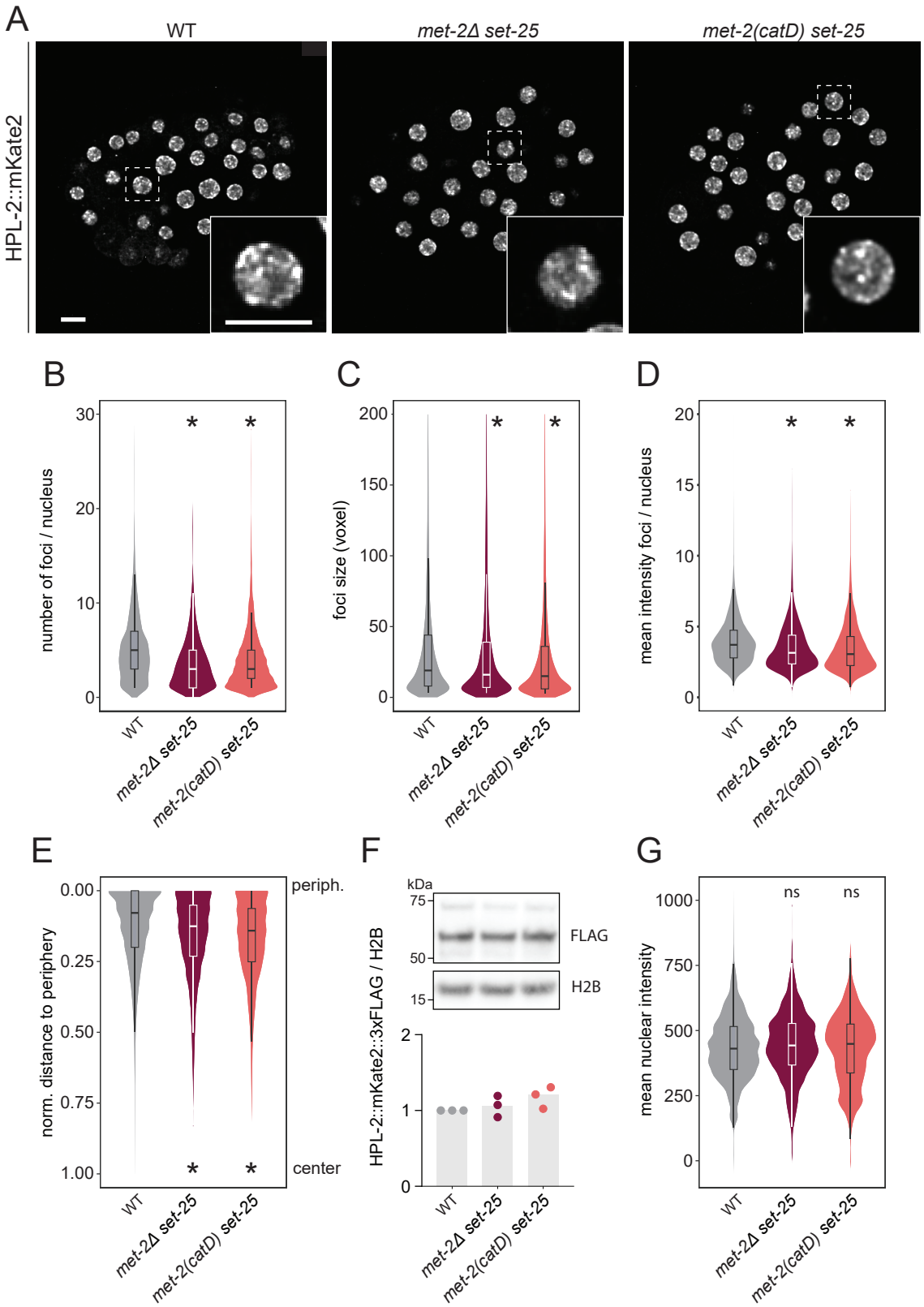

Supplemental Figure S3: MET-2 foci are independent of HPL-2

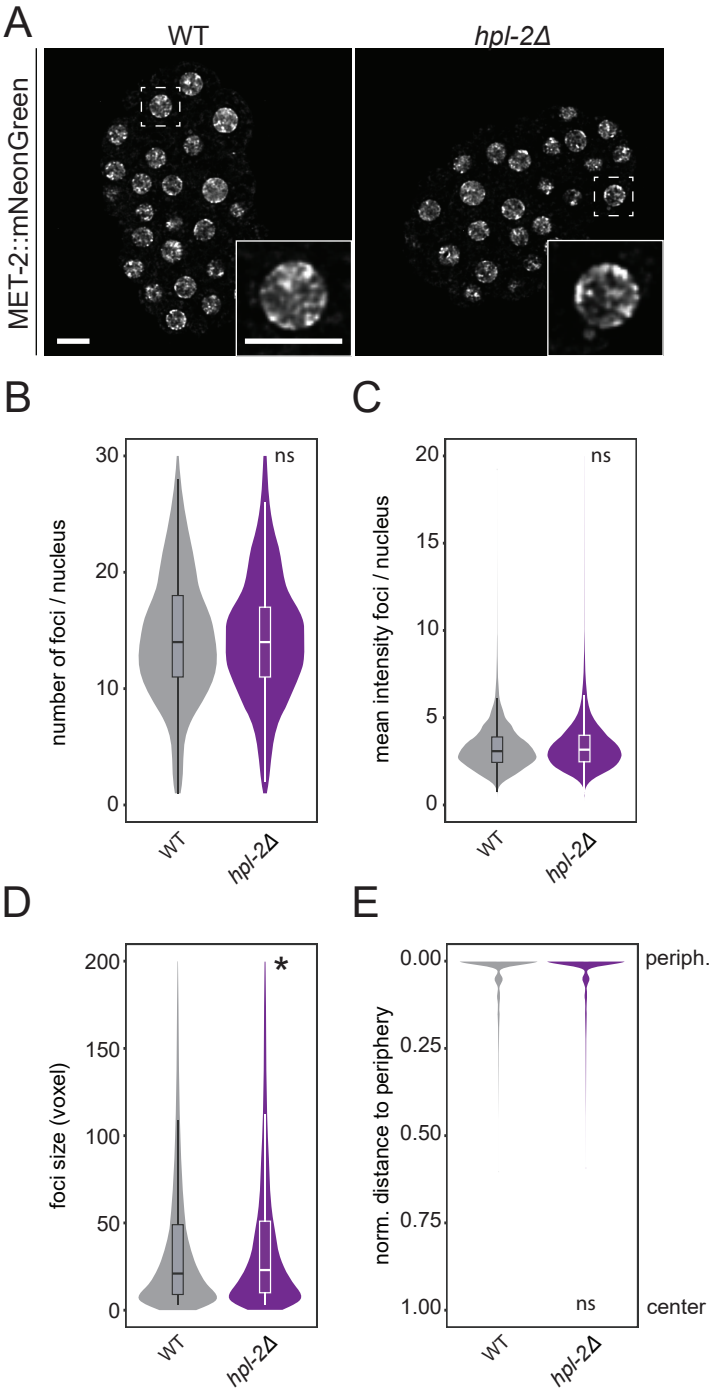

Figure 04: HPL-2 defective in binding H3K9me2/3 represses transcription, forms foci, and supports cell identity commitment

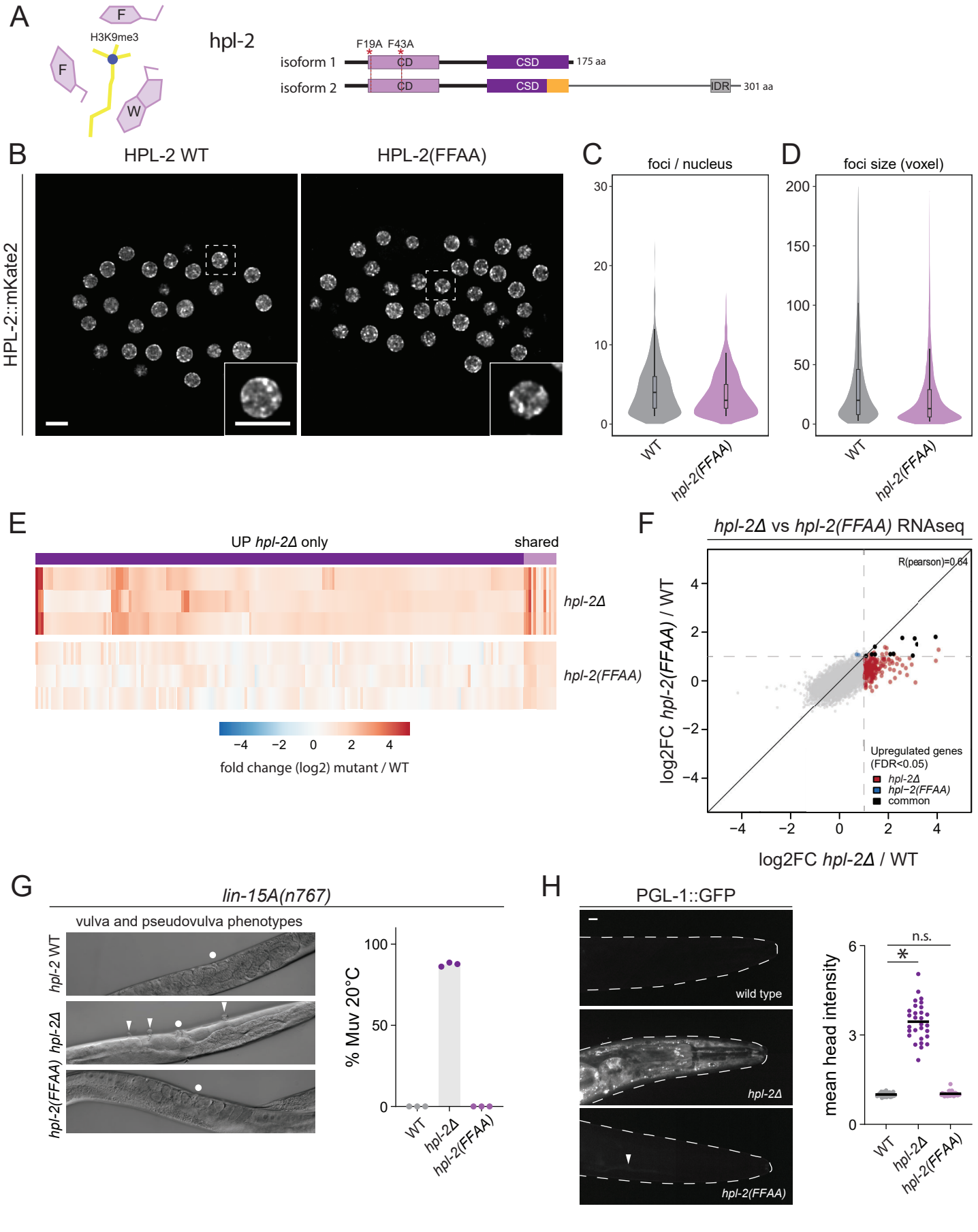

Supplemental Figure S4: Mutation of HPL-2 CD does not alter repression or focus formation

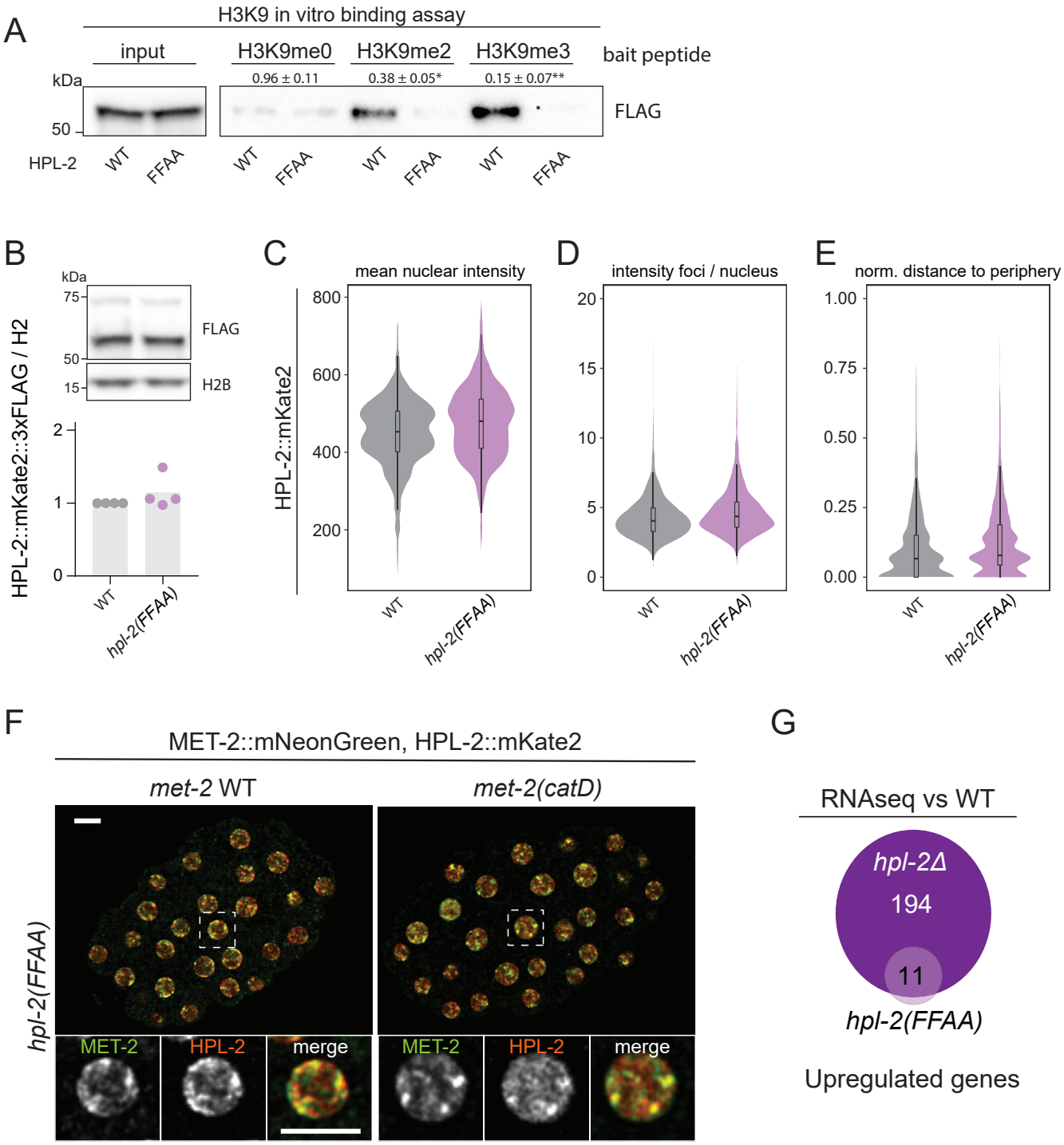

Figure 05: LIN-65, but not MET-2 catalytic activity, is needed for focus formation, repression and cell fate commitment

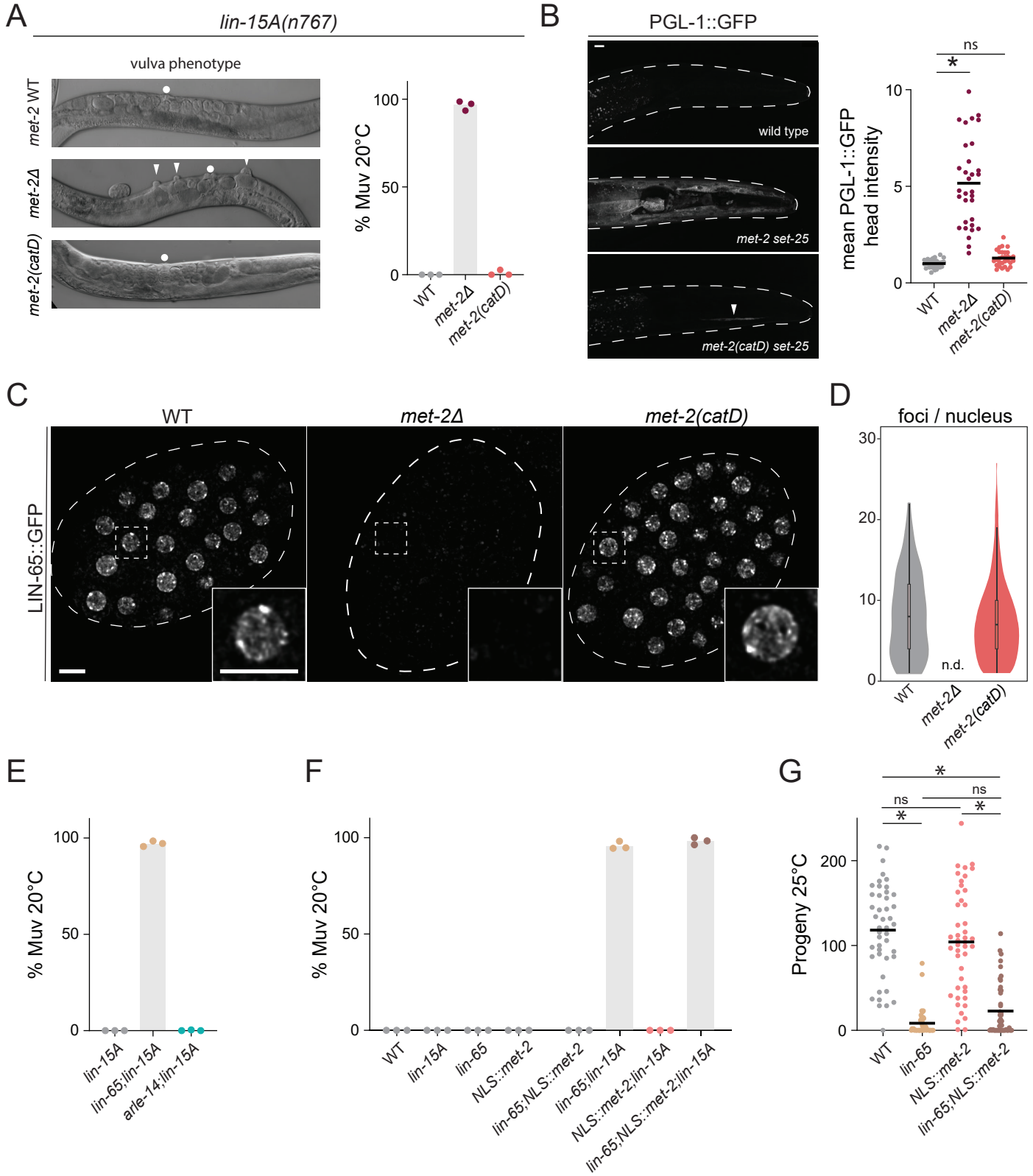

Figure 06: HPL-2 requires physical interaction with the Zn-finger protein LIN-13 to promote cell fate restriction

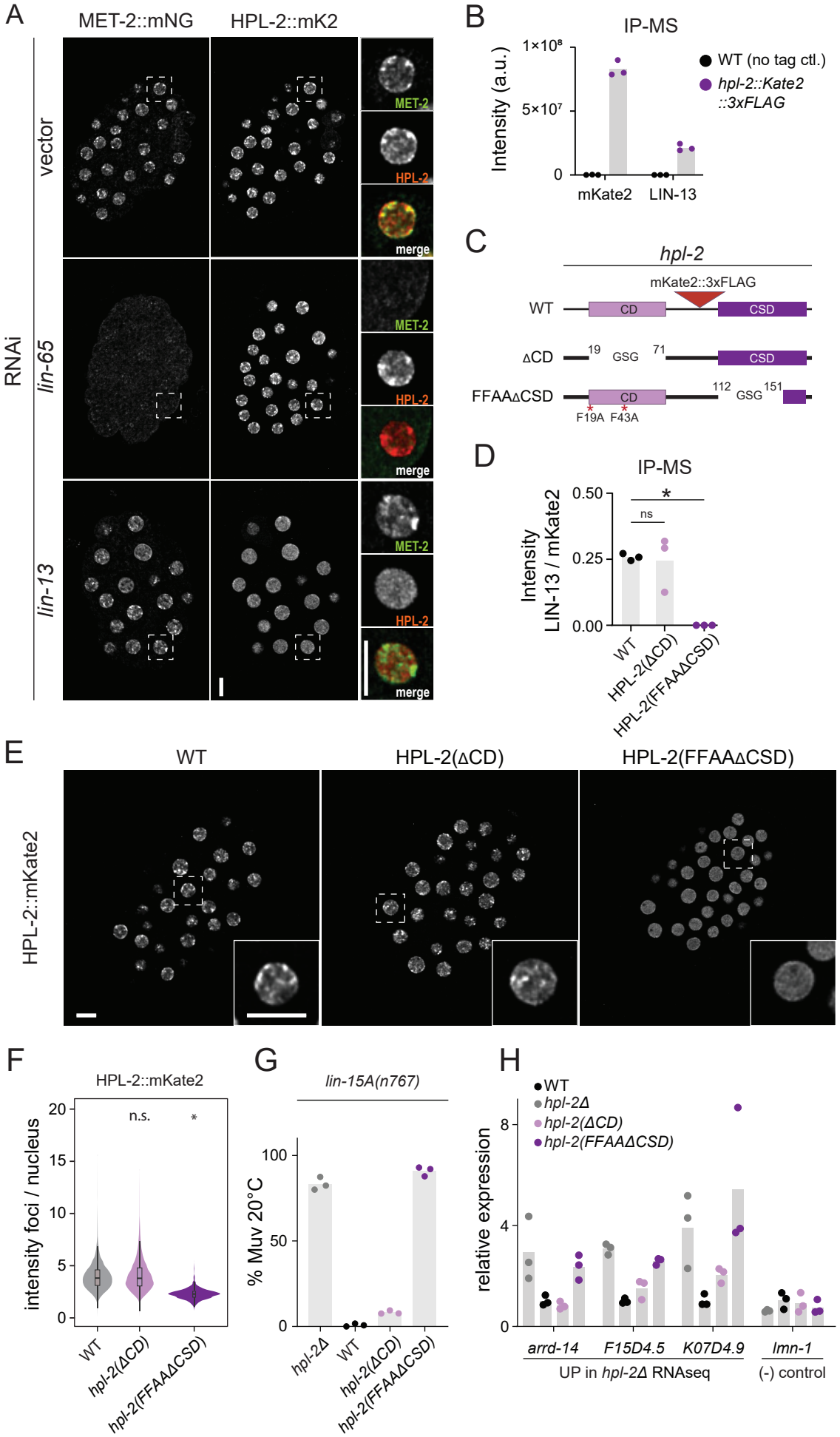
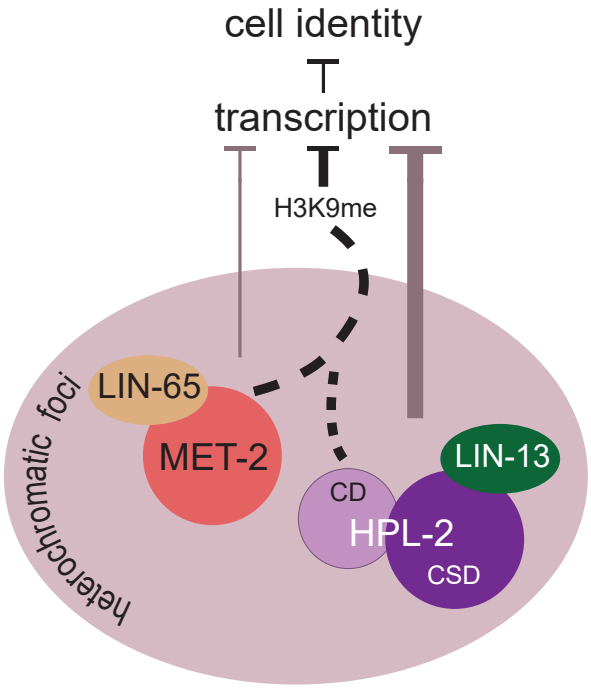
Figure 07: Summary of pathways of repression identified for the H3K9me reader and writer, HPL-2 and MET-2, in cell fate determination